

# REPORT DOCUMENTATION PAGE

AFRL-SR-BL-TR-00-

Public reporting burden for this collection of information is estimated to average 1 hour per response, including the time for reviewing instructions, searching existing data sources, gathering and maintaining the data needed, and completing and reviewing this collection of information. Send comments regarding this burden to Department of Defense, Washington Headquarters Services, Directorate for Information Operations and Infrastructure, Information and Personnel Management Division, Suite 1204, Arlington, VA 22202-4302. Respondents should be aware that notwithstanding any other provision of law, no person's information if it does not display a currently valid OMB control number. PLEASE DO NOT RETURN YOUR FORM TO THE AGENCY.

ding  
ay.  
on of

*0672*

1. REPORT DATE (DD-MM-YYYY) 01-12-2000		2. REPORT TYPE Final Technical Report		3. DATES COVERED (From - To) 01-06-1997 to 31-05-2000	
4. TITLE AND SUBTITLE  Conducting Polymers for Corrosion Control of Coated Aircraft				5a. CONTRACT NUMBER	
				5b. GRANT NUMBER F49620-97-1-0376	
				5c. PROGRAM ELEMENT NUMBER	
				5d. PROJECT NUMBER 3484	
				5e. TASK NUMBER YS	
				5f. WORK UNIT NUMBER	
7. PERFORMING ORGANIZATION NAME(S) AND ADDRESS(ES)  <sup>1</sup> Department of Chemistry <sup>2</sup> Department of Polymers and Coatings North Dakota State University, Fargo, ND 58105-5516 <sup>3</sup> Director, Intelligent Polymer Research Institute University of Wollongong, Wollongong NSW 2522, Australia				8. PERFORMING ORGANIZATION REPORT NUMBER	
9. SPONSORING / MONITORING AGENCY NAME(S) AND ADDRESS(ES)  AFOSR (Air Force Office of Scientific Research) 801 North Randolph St. Room 732 Arlington, VA 22203-1977				10. SPONSOR/MONITOR'S ACRONYM(S) AFOSR/NL	
				11. SPONSOR/MONITOR'S REPORT NUMBER(S)	
12. DISTRIBUTION / AVAILABILITY STATEMENT					
APPROVED FOR PUBLIC RELEASE: DISTRIBUTION UNLIMITED					
13. SUPPLEMENTARY NOTES					
14. ABSTRACT  Chromate surface treatments and chromate-containing epoxy primers are often used for corrosion control of aluminum alloys. However, due to environmental concerns and adverse health effects surrounding such use of chromates, there is an intensive effort to find suitable replacements for chromate-based coatings. Electroactive conducting polymers (ECPs) continue to be of considerable interest as components of corrosion-resistant coating systems. ECPs, in addition to being conductive, are redox active materials, with potentials that are positive of iron and aluminum. Thus, as with chromate, interesting and potentially beneficial interactions of ECPs with active metal alloys are anticipated. Our group has been investigating several ECPs for their corrosion protective properties, with emphasis on solution processable polymers.					
In this final report, the results of long-term immersion, preliminary results of Prohesion® exposure studies, and scanning vibrating electrode technique (SVET), also known as the current density probe (CDP), are described. The coating systems studied incorporated either poly (3-octyl pyrrole) (POP) or poly (3-octadecyl pyrrole) (PODP) as a primer coating of 2 to 3µm thickness. Samples were also studied that utilized a polyurethane topcoat of ca. 20µm thickness in conjunction with the ECP coating. In control experiments, a chromated-epoxy primer of 20µm thickness replaced the ECP coating. The immersion solution for the aluminum 2024-T3 samples was dilute Harrison solution, consisting of 0.35 % (NH <sub>4</sub> ) <sub>2</sub> SO <sub>4</sub> and 0.05 % NaCl. For the cold rolled steel samples a 3% NaCl electrolyte was used for this study.					
15. SUBJECT TERMS Polypyrrole, Corrosion, Aluminum, Electrochemical Impedance Spectroscopy, Electrochemical Noise Method, Polarization Scans, Scanning Vibrating Electrode Technique					
16. SECURITY CLASSIFICATION OF:  a. REPORT Unclas b. ABSTRACT Unclas c. THIS PAGE Unclas			17. LIMITATION OF ABSTRACT	18. NUMBER OF PAGES 45	19a. NAME OF RESPONSIBLE PERSON Dr. Dennis E. Tallman 19b. TELEPHONE NUMBER (include area code) 701-231-8696

## Final Technical Report

### Study of Electroactive Polymers as Corrosion Inhibitors of Aluminum 2024-T3 and Cold Rolled Steel

Dennis E. Tallman,<sup>1</sup> Gordon P. Bierwagen,<sup>2</sup> Gordon G. Wallace,<sup>3</sup>  
Chur Vang,<sup>2</sup> Victoria Johnston Gelling,<sup>1</sup> and Jie He<sup>1</sup>

<sup>1</sup>Department of Chemistry

<sup>2</sup>Department of Polymers and Coatings

North Dakota State University, Fargo, ND 58105-5516

<sup>3</sup>Director, Intelligent Polymer Research Institute

University of Wollongong, Wollongong NSW 2522, Australia

#### ABSTRACT

Chromate surface treatments and chromate-containing epoxy primers are often used for corrosion control of aluminum alloys. However, due to environmental concerns and adverse health effects surrounding such use of chromates, there is an intensive effort to find suitable replacements for chromate-based coatings. Electroactive conducting polymers (ECPs) continue to be of considerable interest as components of corrosion-resistant coating systems. ECPs, in addition to being conductive, are redox active materials, with potentials that are positive of iron and aluminum. Thus, as with chromate, interesting and potentially beneficial interactions of ECPs with active metal alloys are anticipated. Our group has been investigating several ECPs for their corrosion protective properties, with emphasis on solution processable polymers.

In this final report, the results of long-term immersion, preliminary results of Prohesion® exposure studies, and scanning vibrating electrode technique (SVET), also known as the current density probe (CDP), are described. The coating systems studied incorporated either poly (3-octyl pyrrole) (POP) or poly (3-octadecyl pyrrole) (PODP) as a primer coating of 2 to 3 µm thickness. Samples were also studied that utilized a polyurethane topcoat of ca. 20 µm thickness in conjunction with the ECP coating. In control experiments, a chromated-epoxy primer of 20 µm thickness replaced the ECP coating. The immersion solution for the aluminum 2024-T3 samples was dilute Harrison solution, consisting of 0.35 % (NH<sub>4</sub>)<sub>2</sub>SO<sub>4</sub> and 0.05 % NaCl. For the cold rolled steel samples a 3% NaCl electrolyte was used for this study.

**Keywords:** Polypyrrole, Corrosion, Aluminum, Electrochemical Impedance Spectroscopy, Electrochemical Noise Method, Polarization Scans, Scanning Vibrating Electrode Technique

#### DISTRIBUTION STATEMENT A

Approved for Public Release  
Distribution Unlimited

20010102 052

## INTRODUCTION

The use of chromates for corrosion inhibition of metal substrates has come under scrutiny. Due to the environmental concerns and adverse health effects surrounding such use of chromates, there is an intensive effort to find suitable replacements for chromate-based coatings. While the search for a chromate replacement is underway<sup>1</sup>, more efforts have focused on the use of electroactive conducting polymers (ECPs) as components of corrosion resistant coating systems. This is due, in part, to the conductivity as well as the redox activity these materials exhibit, with typical potentials positive of aluminum.<sup>2</sup>

Starting with Deberry's<sup>3</sup> work a noted effort has been seen in probing the corrosion inhibition provided to steel<sup>4,5,6,7,8,9,10,11,12,13,14</sup> and aluminum<sup>15,16,17,18,19</sup> by polyaniline. However, polypyrrole has received relatively little attention. The research involving polypyrrole has mainly focused on films that were electrochemically deposited onto steel. There appears to be little or no reported work involving polypyrrole on aluminum alloys or steel.<sup>20,21,22,23,24,25</sup> One of the factors affecting the inquiries into the corrosion inhibition provided by polypyrrole is the relatively low solubility. Polypyrrole films also tend to have poor mechanical properties. Steps have been taken to increase both the solubility and mechanical properties; however, modification of the polymer usually results in a decreased conductivity. A novel approach to increase both the solubility and processibility of polypyrrole has been to add organic substituents to the pyrrole ring.<sup>26,27</sup> The result is a polymer soluble in common organic solvents in which the polymer brittleness is ameliorated by the alkyl side groups.

In this work, electrochemical impedance spectroscopy (EIS), electrochemical noise methods (ENM), polarization methods, and scanning vibrating electrode technique (SVET) was utilized to examine the interactions of polypyrrole with aluminum alloy 2024-T3 and cold rolled steel. The corrosion protection provided by a polypyrrole/polyurethane two-coat system was also evaluated using EIS during both long-term immersion and prohesion exposure experiments. Two variations of polypyrrole were studied, poly(3-octyl pyrrole) (POP) and poly(3-octadecyl pyrrole) (PODP). The ECPs were applied as a primer coating of 2 to 3- $\mu\text{m}$  thickness, with a polyurethane topcoat of ca. 20- $\mu\text{m}$  thickness. In control experiments, a chromated-epoxy primer of 20- $\mu\text{m}$  thickness replaced the ECP coating. The immersion solution for the aluminum 2024-T3 samples was dilute Harrison solution, consisting of 0.35 %  $(\text{NH}_4)_2\text{SO}_4$  and 0.05 % NaCl. For the cold rolled steel samples a 3% NaCl immersion electrolyte was used.

## EXPERIMENTAL

**Sample Preparation.** The poly(3-octyl pyrrole) and poly(3-octadecyl pyrrole) were synthesized electrochemically by the Intelligent Polymer Research Institute (Wollongong, Australia) and contained perchlorate and paratoluene sulfonate counterions (Figure 1). The synthetic details and polymer characterization have been described elsewhere.<sup>27</sup> In short, the polymers were generated galvanostatically at a platinum electrode at a current density of 1 mA/cm<sup>2</sup> from a solvent mixture of CCl<sub>4</sub> (80%) and

$\text{CH}_2\text{Cl}_2$  (20%) containing 0.1 M monomer (3-octyl pyrrole or 3-octyldecyl pyrrole), 0.1 M tetrabutylammonium perchlorate and 0.025 M tetrabutylammonium *p*-toluenesulfonate. The soluble fraction of the electrosynthesized polymer was recovered from the liquor and excess electrolyte removed. Cast films of the polymers were both electroactive (by cyclic voltammetry) and conductive (ca.  $5 \times 10^{-3}$  S/cm for POP and 30 S/cm for PODP; both by 4-point probe method).

The cold-rolled steel (Q-Panel), aluminum alloy (Al 2024-T3, Q-Panel) and pure aluminum (99.998%, Alfa Aesar) substrates were first polished using 600 grit silicon carbide, washed with hexane, and air-dried. After this pretreatment, the POP or PODP coating was applied by solution casting from a 1% solution in a solvent consisting of 50%  $\text{CCl}_4$  and 50%  $\text{CH}_2\text{Cl}_2$ . The coatings were allowed to dry overnight. The average coating thickness was  $2.3 \pm 1.6 \mu\text{m}$ .

Top coated samples for the long-term immersion and Prohesion® studies were coated by drawdown bar method with a DEFT® high gloss 2-K polyurethane. The thickness of the topcoat was 20-30  $\mu\text{m}$ . Samples were also prepared that served as a standard. These samples consisted of a chromated epoxy primer (DEFT®) of a thickness of approximately 20  $\mu\text{m}$  and the polyurethane topcoat of a thickness of 20-30  $\mu\text{m}$ .

### Instrumentation and Experimental Conditions.

The SVET instrumentation used in these experiments was from Applicable Electronics (Forestdale, MA) and is described in detail elsewhere. Scanning electron microscopy (SEM) and energy dispersive X-ray (EDX) analysis of Al 2024-T3 samples were performed with a JEOL JSM-6300V microscope (JEOL LTD., Tokyo, Japan) equipped with a Noran Voyager II EDX analysis system (Madison, Wisconsin). An accelerating voltage of 15 kV, a take-off angle of 29.0° and a 100-sec. count were used.

Samples were prepared for SVET measurement by cutting into 1-cm x 1-cm squares and masking by a Polyester 5 adhesive tape (3M Company) such that only a 2-mm x 2-mm square opening of the sample was exposed. The POP coating of each sample was scribed to introduce a defect extending to the metal surface, the area of the defect ranging from 0.1 to 0.3  $\text{mm}^2$  (epoxy-coated control samples were scribed in the same manner). The sample was mounted in a Teflon sample cell and the appropriate immersion solution (ca. 5-mL) was added. The immersion solution for the Al 2024-T3 samples was dilute Harrison solution ( $0.35\% (\text{NH}_4)_2\text{SO}_4$ , 0.05% NaCl in  $\text{H}_2\text{O}$ ). The immersion solution for the cold-rolled steel samples was 3% NaCl solution. These solutions were prepared from reagent grade salts and distilled water.

Scans were initiated within 5 minutes of immersion and were collected every 20 minutes for the duration of the experiment, typically 20 hours. Each scan consisted of 400 data points obtained on a 20 x 20 grid, with an integration time of 1-second per point. A complete scan required 10 minutes, followed by a 10-minute rest period prior to the next scan. The current density maps are displayed in two ways. In one method, the normal or z-component of the measured current density in the plane of the vibrating

electrode is plotted in 3-dimensional format over the scan area, with positive and negative current densities representing anodic and cathodic regions, respectively. In the other method, vectors representing current density magnitude and direction are superimposed onto an optical image of the immersed sample. In all cases, the bottom edge of the optical micrograph corresponds to the x-axis of the 3-dimensional plot. The measurements were taken at the open-circuit potential. At least six specimens of each sample type were prepared and scanned to assess reproducibility of the observed phenomena. In each case, representative scans are presented.

Electrochemical Impedance Spectroscopy (EIS) was employed in the long-term immersion studies as well as the samples placed in the Prohesion® cabinet. The EIS was performed using a three-electrode configuration. The reference electrode was a saturated calomel electrode (SCE) and the counter electrode consisted of a platinum mesh electrode. The electrolyte solution used as the immersion and Prohesion® solution was dilute Harrison solution (0.35 %  $(\text{NH}_4)_2\text{SO}_4$ , 0.05% NaCl in H<sub>2</sub>O). The solution was prepared from reagent grade salts and Milli-Q® water. A polyvinyl chloride (PVC) pipe was glued, using marine quality adhesive, onto the coated surface to serve as a reservoir for the electrolyte solution. EIS instrumentation consisted of a PC3 (or PC4) potentiostat in addition to an 8-channel multiplexer controlled by CMS100/300 software (Gamry Instruments). Impedance measurements were carried out at the open circuit potential with a 5 mV amplitude perturbation over the frequency range of 5000 Hz to 0.01 Hz.

Electrochemical Noise Method (ENM) studies were performed using a Gamry PC3 in conjunction with an 8-channel multiplexer run by CMS100 software. The sample setup was similar to the EIS experiments except that two nominally identical panels were needed. The samples used for the ENM experiments consisted of only the ECP of interest, i.e. no polyurethane topcoat was employed in this study. These panels functioned as the working electrodes and were connected together both electrolytically via a 0.6 N NaCl Agar salt bridge and electrically, via a zero resistance ammeter. Along with the two working electrodes and salt bridge, a saturated calomel electrode was used as the reference electrode. At designated time intervals the samples were each monitored for 256 seconds. During the sample measurement both the instantaneous current and potential were recorded at 0.5 Hz. From the 128 values of current and potential recorded, the mean current,  $I_m$ , and mean potential,  $V_m$ , and the standard deviations of each,  $\sigma_I$  and  $\sigma_V$ , were calculated for the observation time. From these values the noise resistance,  $R_n = \sigma_V/\sigma_I$ , was calculated.<sup>28</sup>

Polarization scans were performed using a Gamry potentiostat PC4 controlled by CMS100 software. The electrochemical cell setup was identical to that of the EIS setup described above, with the reference electrode consisting of a saturated Calomel electrode and a platinum counter electrode. The potential range was from -0.25 V to 0.5 V versus the open circuit potential (Eoc) at a scan rate of 5 mV/sec. Dilute Harrison solution was used as the electrolyte solution. Samples were coated with the ECP of interest using the same procedure described above, however no polyurethane topcoat was employed. A scribe was created to produce a defect with a length of 2 cm with an overall defect area of 0.035 cm<sup>2</sup>.

## RESULTS AND DISCUSSION

**The Mapping of Current Density.** The electrochemical techniques commonly used in corrosion studies (for example, linear polarization, electrochemical impedance spectroscopy, or electrochemical noise methods) provide data that reflect an average response over the entire sample surface. While such data is very useful, no local or spatial information is obtained. A number of techniques have been developed recently which permit mapping of local current flows in the electrolyte above an immersed substrate, providing a more detailed view of corrosion processes. Typically, these techniques map the local potential field that arises due to current flow through the resistive electrolyte and the potential map is then converted to a current density map by a calibration process.

The scanning reference electrode technique (SRET) as originally implemented maps the potential by scanning two micro-reference electrodes near the surface of the substrate under immersion.<sup>29</sup> More recent versions of the SRET use a single vibrating microelectrode, leading to improvements in spatial resolution.<sup>30</sup> This technique is often referred to as the scanning vibrating electrode technique or SVET, although there are several variations in how the electrode is actually vibrated.<sup>30</sup> These techniques are limited to measuring DC currents which restricts their application to the study of bare metal substrates or coated-metals having coating defects<sup>31,32</sup>.

Local electrochemical impedance spectroscopy (LEIS) utilizes a twin microelectrode probe to measure the AC current flowing near the surface of a substrate that results from an AC potential perturbation applied to the substrate.<sup>33</sup> Thus, LEIS is applicable to both bare and coated metals under immersion,<sup>34,35</sup> but the requirement of a twin microelectrode probe sacrifices some spatial resolution. Recent variations of the SVET permit local impedance measurements using the single vibrating electrode.<sup>36,37</sup>

**Control Experiments.** In this work, the current density in and around a defect in a chromated-epoxy coating applied either to cold-rolled steel (and immersed in 3% NaCl) or to aluminum 2024-T3 (and immersed in dilute Harrison solution) was studied using the SVET. Control experiments involving bare cold-rolled steel and bare Al 2024-T3 in the corresponding immersion solutions were also conducted. In every case, these bare metals exhibited one or more (in the case of the Al alloy, typically several) regions of anodic activity, reflecting sites of localized corrosion, with current densities of 100-200  $\mu\text{A}/\text{cm}^2$ . With steel, the corrosion often continued until the build-up of corrosion products at a particular site led to a crash of the scanning probe. With Al 2024-T3, the activity was much more dynamic, with anodic sites appearing (onset of pitting corrosion) and then disappearing (passivation) on a time scale of tens of minutes. Of importance to the following discussion is the observation that corrosion onset at these bare metal samples was virtually immediate, with the observation of significant current flow during the first SVET scan, which was initiated within 5 min. of immersion.

As an additional control experiment, current density maps were obtained for steel and Al alloy samples coated with a plain (nonchromated) epoxy primer. A defect was

introduced by scribing through the coating to the bare metal surface. The results of these experiments are exemplified by the result for steel shown in Figure 2. Clearly visible in the micrograph of Figure 2 is the 2-mm by 2-mm scan area defined by the Polyester 5 adhesive tape. The defect, which is parallel to the X-axis, is visible within this scan area. From Figure 2, it is clear that the major current flow is from a single anodic site to a single cathodic site, each located within the defect. This confirms that the coating is effectively removed by scribing, exposing the bare metal. In every such control experiment for steel and aluminum, similar behavior was observed, with oxidation and reduction currents confined to the defect. With steel, the onset of corrosion within the defect was very rapid, typically observed in the first scan (i.e., within 5 min.). With aluminum, the onset of corrosion within the defect was somewhat more variable, but was typically observed by the second scan (i.e., within 20 min.). For the steel sample of Figure 2, the current slowly diminished toward zero over the course of approximately 3.5 hours, at which point the leftmost two-thirds of the defect area was covered with corrosion product (Figure 3). The cathodic site remained free of corrosion product throughout the experiment.

We note that Kinlen<sup>38</sup> and coworkers recently conducted a similar SRET experiment at epoxy coated carbon steel with a 1-mm diameter pinhole drilled through the coating to the metal surface. They also observed anodic and cathodic reactions occurring within the defect. The onset of corrosion was immediate and the corrosion rate did not appear to diminish over the 8-hour duration of the experiment.

**Chromated-Epoxy Primer on Steel.** Two differences were observed in the experiments involving chromated-epoxy primer on steel. First, whereas large currents were observed within 5-minutes in the control experiments, there was a significant delay of 40-minutes or longer before the onset of any observable corrosion current in these experiments. Second, significant reduction current on the exposed metal in the defect, as always observed in the control experiments, was not observed in these experiments.

Figure 4 shows a sample after 169-minutes of immersion (the first observable current for this particular sample was at 42-minutes immersion). Oxidation was clearly occurring within the defect and corrosion product is visible at the anodic site in the optical micrograph. However, little if any reduction occurred within the defect. Rather, reduction appeared to occur more or less uniformly across the coating surface. Since the reduction current was spread out over a relatively large area, the current density at any one point was rather small, similar in magnitude to the noise level. Therefore, we repeated this experiment eight times to confirm this general behavior. In every case the surface of the coating was uniformly depressed below zero current (i.e., uniformly cathodic), with little or no reduction current within the defect. With the plain epoxy control experiments, the total anodic current and total cathodic current flowing above the defect were approximately equal. In these chromated-epoxy experiments, the anodic current was always greater. We conclude that reduction in these experiments did indeed occur over the chromated-epoxy coating.

There are two reduction mechanisms that might explain these observations. In one mechanism, the reduction reaction could occur at the coating-electrolyte interface, with electron transfer to the underlying metal mediated by the chromate pigment in the epoxy coating. In the other mechanism, the reduction reaction could occur at the metal-coating interface, the result of diffusion of the oxidant through the coating to the metal surface. Both mechanisms would give rise to a cathodic current flow above the coating surface.

We favor the first mechanism for the following reasons. First, the reduction current always appeared to be rather uniformly distributed across the coating surface. Reduction at the metal-coating interface would likely be more localized, with transport (e.g., of oxygen) to the metal interface occurring primarily through coating defects. Second, the first occurrence of observable oxidation within the defect at ca. 40 min. is accompanied by uniform reduction over the coating surface, a time we consider too short for uniform penetration of water and oxidants through the coating to the metal interface.<sup>39</sup> It is noted, however, that the pigment volume concentration of this highly pigmented primer (ca. 40-45%)<sup>40</sup> is close to the critical pigment volume concentration (ca. 50%), and pathways of conductivity due to electrolyte channels may form in the partial porosity that occurs in such coatings.<sup>41</sup> Finally, if the mechanism involves simple diffusion through the coating and reduction at the underlying metal, then similar behavior might be expected for an aluminum alloy. However, at aluminum alloy the reduction occurs preferentially within the defect (see next section). This suggests a more metal specific mechanism, such as might occur if coupling of electron transfer between metal and coating were involved.

If reduction is occurring at the coating-electrolyte interface, the implications are two-fold. First, the chromated-epoxy coating must be capable of shuttling electrons from the metal to an oxidant in solution. That is, the coating would need to be electronically conducting or semi-conducting. The mechanism of conduction in this coating is not clear, but could involve electron transfer between contacting chromate particles within the coating, similar to that occurring in redox polymers such as poly(vinylferrocene).<sup>42</sup> Experiments are underway to assess the conductivity of the chromated-epoxy coating. Second, cathodic delamination of a coating is generally associated with a high local hydroxide concentration generated by the reduction reaction occurring at the coating-metal interface.<sup>43,44</sup> Removal of the reduction reaction from the metal interface may be an important aspect of the mechanism by which chromated-coatings extend the lifetime of the complete coating system. A mechanism of this type has been proposed for conducting polymers<sup>45</sup> and, indeed, reduction reactions at poly(3-octyl pyrrole)<sup>46</sup> coatings and at polyaniline coatings<sup>38</sup> on steel have been observed.

In these experiments, we observed no tendency for the chromated-epoxy primer to rapidly passivate the steel. In fact, once corrosion current began to flow (following the initial delay), it continued for 18 to 20 hours, until corrosion products eventually covered the anodic site and diminished the current to near background levels. In contrast, the current at plain epoxy coated steel diminished after only 3 to 4 hours (Figure 3). This suggests that the presence of the oxidant (chromate) in the epoxy primer actually sustains

the current under our immersion conditions. Very similar behavior was observed for a polypyrrole coating (also an oxidant) on steel.<sup>46</sup> An additional observation may be relevant here. The corrosion products formed at the defect of the plain epoxy coated steel appeared to be more voluminous and less adherent, with considerable suspended matter forming in the immersion solution during the course of the experiment. On the other hand, the products formed at the defect of the chromated-epoxy coated steel appeared to be much more adherent, with little or no suspended material appearing in the immersion solution in spite of the considerably greater time over which oxidation occurred.

An insulating topcoat such as polyurethane would be expected to block the reduction reaction observed at the chromated-epoxy coating surface, forcing the reduction process to occur at the defect. In preliminary experiments with chromated-epoxy samples prepared as described previously but with a ca. 50- $\mu\text{m}$  thick polyurethane topcoat and a defect introduced through both coatings to the metal surface, the oxidation and reduction reactions were indeed confined to the defect. Importantly, there was still a delay of approximately 1-hour before observation of any redox activity, a delay similar to that observed without the topcoat. Further studies of topcoated substrates are in progress.

**Chromated-Epoxy Primer on Al 2024-T3.** The chromated-epoxy primer on Al 2024-T3 alloy, as on steel, significantly retarded the onset of corrosion. Whereas corrosion activity was observed within ca. 20 min. for the plain epoxy control samples, the first detectable current with the chromated-epoxy samples was typically after 5-hours of immersion. The results are exemplified by Figure 5, which shows the current density maps for a particular sample after 5-minutes immersion and after 5.5-hours immersion. The 5-minute map is typical of those obtained over the first 5-hours of immersion, showing no detectable corrosion of the metal exposed in the defect. The exposed metal in the defect remained shiny during this period. The first sign of corrosion is displayed in the 5.5-hour map (Figure 5), with both oxidation and reduction being confined to the defect area. As with the steel samples, this corrosion current continued to increase over the next several hours of immersion, and most of the exposed metal area in the defect turned dark in color. Figure 6 shows the current density maps for the same sample after 17.5-hours immersion, by which time the current had increased substantially but still appeared to be confined to the defect area. Two local cathode sites, one on each side of the anode site, are observed. As noted in the previous section, this behavior is in contrast to that on steel where cathodic currents above the coating were observed. The site of corrosion is clearly visible in Figure 6 as the remaining shiny metal spot in the micrograph.

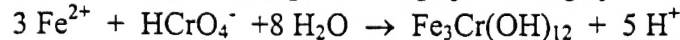
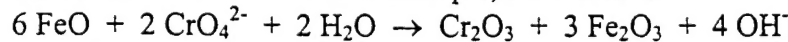
Long-term immersion experiments were conducted to determine the time required for the corrosion current to diminish to background levels. For the plain epoxy control experiment, the average time required was approximately 16 hours. For the chromated-epoxy coated samples, the average time required was greater than 24 hours. As for steel, the presence of the oxidant chromate appeared to sustain the corrosion current.

In a related study, the SRET was used to investigate a scratched chromated-epoxy primer on galvanized steel immersed in an artificial acid rain solution.<sup>47</sup> In that work, as

in this, the chromate-containing epoxy coating delayed the onset of corrosion within the defect compared to a chromate-free epoxy coating. Once corrosion ensued, the chromated-epoxy sample displayed a more rapid passivation, requiring 2-3 days under their immersion conditions. It was suggested that the chromated-epoxy coating released chromate ions into the defect site, promoting passivation of the exposed metal. However, except at very low pH, the leaching of chromate from epoxy coatings appears to be a relatively slow process.<sup>47,48</sup> Such a process probably plays only a minor role over the time course of our experiments, which typically are 20-30 hours in duration. It is also possible that the mechanical scribing technique used in these studies embeds or otherwise deposits chromate pigment particles within the defect area, influencing behavior during early immersion stages.

**Mechanisms of Chromate Inhibition.** The detailed mechanisms by which Cr<sup>6+</sup> (either CrO<sub>4</sub><sup>2-</sup> or Cr<sub>2</sub>O<sub>7</sub><sup>2-</sup>, depending on concentration and pH) decreases the corrosion rate of Fe and Al alloys are still unclear. Chromate-containing coatings have the reputation of protecting these alloys from corrosion, especially in damaged areas of the coating system (such as the defects introduced into the coatings used in this work).<sup>49,50</sup> Clearly the oxidizing power of CrO<sub>4</sub><sup>2-</sup> is important and several redox reactions are possible, including direct oxidation of metal substrates.<sup>51,52</sup> In these processes, the Cr<sup>6+</sup> is reduced to Cr<sup>3+</sup> and, as a consequence, composite oxide/hydroxide adherent films are formed with the general composition x•M<sub>2</sub>O<sub>3</sub>/y•Cr<sub>2</sub>O<sub>3</sub> or x•M(OH)<sub>3</sub>/y•Cr(OH)<sub>3</sub>, where M is Fe or Al and x and y are variable, depending on conditions.<sup>53</sup> The negative charge on CrO<sub>4</sub><sup>2-</sup> (or Cr<sub>2</sub>O<sub>7</sub><sup>2-</sup>) facilitates migration of Cr<sup>6+</sup> to anodic sites where such passivation processes occur.<sup>54</sup> Furthermore, chromate at low concentrations is also known to function as a cathodic inhibitor for both Fe<sup>55</sup> and Al 2024-T3.<sup>56</sup> As noted in the previous section, low concentrations of CrO<sub>4</sub><sup>2-</sup> in the defect are expected during the initial stages of immersion and these mechanisms may play a role in the initial delay to the onset of corrosion<sup>53</sup> observed at both alloys of this work.

The sustained oxidation current observed (after the initial delay) at the defect on chromated-epoxy-coated steel and the apparent alteration of corrosion products noted earlier is consistent with the observation that, typical of chromate-inhibited iron corrosion, Fe<sup>2+</sup> is further oxidized to Fe<sup>3+</sup>. For example, the reactions



have been identified under near neutral pH conditions<sup>57,58</sup>, resulting in the formation of more adherent composite oxide/hydroxide films with enhanced resistance to dissolution.

Similarly, the formation of composite oxide/hydroxide films are believed to play an important role in the chromate inhibition of aluminum alloys<sup>53,54</sup>, although the composition of such films are have only recently been examined in detail.<sup>56,59</sup> As for steel, the sustained oxidation current in the presence of chromate may ultimately lead to a passive film of different composition and perhaps more resilience than that produced in the absence of chromate. For example, the increased time to passivation may allow for diffusion/migration of Cr<sup>6+</sup> species to the anodic site and subsequent incorporation of Cr<sup>3+</sup> (and perhaps Cr<sup>6+</sup>) into the passive film.<sup>59</sup>

**Poly(3-octyl pyrrole) Coating on Steel.** There are rather striking similarities between the results obtained in this work with the POP coating on steel and the results reported for a chromated-epoxy coating on steel.<sup>60</sup> As was observed with the chromated-epoxy coating, the POP coating delayed the onset of corrosion within the defect. However, the delay was significantly longer, typically ca. 3 hours with the POP coating, compared to ca. 40 minutes for the chromated epoxy coating and virtually no delay for a plain epoxy coating.<sup>60</sup> Figure 7 (top) shows the current density map for POP-coated steel at 5-minutes immersion in 3% NaCl (the optical micrograph for this sample is displayed in Figure 8). No significant current flow was observed and similar inactivity was maintained for ca. 3 hours. Figure 7 (bottom) shows the map recorded at 166-minutes immersion, at which time the first significant current flow was observed. The current increased with time, reaching the maximum (ca. 100  $\mu\text{A}/\text{cm}^2$ ) after 5-hours and 35-minutes immersion (Figure 8). The current then slowly decreased as the defect became covered with a dark deposit of corrosion product, reaching near background levels after ca. 19 hours. As observed for a chromated epoxy coating (but in contrast to a plain epoxy coating),<sup>60</sup> the corrosion product appeared to be adherent, with little or no suspended corrosion product evident in the immersion solution.

In these experiments, the current associated with the defect is always anodic, with two main anodic sites for this particular sample apparent in the current maps of Figure 8. Significant cathodic current was never observed within the defect. Rather, the cathodic current was always distributed more or less uniformly across the conducting polymer surface, as clearly evident from Figure 8. We postulate that oxygen reduction occurs at the POP/electrolyte interface, with electron transfer from the metal to oxygen being mediated by the POP. This process drives the oxidation reaction observed in the defect, which ultimately leads to passivation of the exposed metal within the defect. Of course, the oxidizing potential of POP may be an important factor in this mediation process. Kinlen<sup>38</sup> and coworkers recently reported a similar observation for polyaniline-coated steel where the scanning reference electrode technique revealed localized anodes in pinhole defects and a delocalized cathode spread over the polyaniline surface.

**Poly(3-octyl pyrrole) Coating on Al 2024-T3.** The results obtained for POP on Al 2024-T3 are particularly interesting. In the initial experiments, the defects introduced into the coatings were of dimensions similar to those used for the steel samples (for example, see Figure 8). However, little or no activity was observed with these samples even after many hours of immersion, so the size of the defect was increased. Figure 9 illustrates a typical sample with the larger defect, this optical micrograph and current density map captured at the 5-minute mark. Close examination of the current density map reveals a very small oxidation current flowing at the defect, particularly noticeable at the left edge of the defect, corresponding to the left end of the X-axis and the midpoint of the Y-axis. A correspondingly small reduction current occurs at coated areas of the substrate. Admittedly these currents are near the background level, but may reflect the development of a protective oxide coating at the defect during the early stages of immersion. Even with this rather sizable defect, the current flow typically remained at near background level for over 22 hours. By comparison, sizable current flow (>10

$\mu\text{A}/\text{cm}^2$ ) was observed at chromated-epoxy coatings within ca. 5 hours and at plain epoxy coatings within ca. 20 minutes.<sup>60</sup>

The first significant current flow at this sample was observed after 22-hours, 14-minutes of immersion, shown in Figure 10 (top). However, in contrast to other combinations of coatings and metals we have examined where oxidation always occurred at the defect, the oxidation current in this case appeared to originate at a coated area of the aluminum alloy. The current increased over the next hour during which time the defect area exhibited a rather uniform reduction current (Figure 10). Indeed, from this time of immersion onward, oxidation at the defect was never observed with these samples. The metal within the defect remained shiny throughout the immersion experiment with no visual evidence of corrosion products. To assess the reproducibility of this observation, a total of eight POP-coated samples were examined by the SVET. In every case, the above general behavior was observed, with no significant oxidation occurring at the defect of any of the eight samples. Additionally, there appeared to be no coating defects (e.g., pinholes) that might account for the observed behavior.

The oxidation current observed in Figure 10 continued to increase over the next several hours, reaching the level shown in Figure 11 (top) after 26-hours, 34-minutes immersion. The optical micrograph of Figure 11 (bottom) confirms that the oxidation is occurring at a coated region of the alloy and not at the defect. The current continued to flow for several days, dropping to ca.  $20 \mu\text{A}/\text{cm}^2$  after 5 days, at which point the experiment was terminated and the coating removed by dissolving in chloroform followed by acetone.

The oxidation currents observed in Figures 10 and 11 indicate that anions were moving into (or equivalently, cations out of) the POP coating. There are at least two possible explanations for this observation: either the POP coating itself was oxidized or the aluminum alloy beneath the coating was oxidized. An optical micrograph of the Al 2024-T3 surface after removal of the POP coating is shown in Figure 12. The POP coating has been removed from the 2-mm x 2-mm scan area, but not from the surrounding area protected by the Polyester 5 tape. Visible within this scan area is the original defect (the scribe mark). Also visible (and much more apparent under binocular observation) are pits formed in the alloy surface at the site of the oxidation current (compare the micrographs of Figures 11 and 12). Thus, we conclude that the observed oxidation current was due to the oxidation of the aluminum alloy (i.e., pitting corrosion) beneath the POP coating.

There remains a confounding question. Why does the oxidation of aluminum alloy always occur under the polymer coating and not at exposed metal within the defect as observed for steel? After all, the defect area is exposed directly to the aggressive electrolyte ions, whereas the POP-coated area is not (although exchange of the POP counterions with electrolyte ions likely occurs). One explanation might involve direct oxidation of the metal by the POP with concomitant reduction of the POP. However, such an internal redox reaction would not require charge compensation of the POP from the electrolyte (i.e., there would be no ion flux at the POP surface) and such a process

would not be observed by the SVET. The POP coating may mediate the oxidation of the alloy by shuttling electrons from the alloy to oxygen (or other oxidant) at the POP/electrolyte interface, as observed for steel (Figure 8). Indeed, reduction at the POP/electrolyte interface (as well as in the defect) was often observed with the Al alloy (e.g., see Figure 13). However, the mediation of electron transfer by the POP would not explain the absence of oxidation within the defect and the localized undercoating oxidation.

One possible explanation is that the POP provided a thermodynamic assist to the oxidation of the aluminum alloy by forming stable metal ion complexes with the oxidized metal ions (principally  $\text{Al}^{3+}$  and/or  $\text{Cu}^{2+}$ ). Indeed, a similar mechanism has been suggested for polyaniline on Al 2024-T3, where X-ray photoelectron spectroscopy showed depletion of Cu from the alloy surface by the conducting polymer.<sup>17</sup> As the metal ions enter the POP, charge balance would be maintained by an anion flux from electrolyte into the polymer, resulting in the observed current flow above the polymer surface. A slight color change in the POP coating immediately above and around the site of oxidation was observed (from black to dark blue-green), indicating a localized change in coating composition consistent with this hypothesis. Furthermore, the incorporation of metal ions into polypyrrole by complexation has been reported, both by direct coordination to the pyrrole nitrogen<sup>61</sup> and by incorporation and strong binding (as counterions) of anionic metal complexes.<sup>62</sup>

**Energy-Dispersive X-Ray Analysis.** All POP-coated Al 2024-T3 alloy specimens examined by SVET eventually displayed (after the previously described induction period) localized undercoating corrosion, as exemplified by Figures 11 and 12. Such a localized oxidation process may be related to the known heterogeneous structure of the aluminum alloy surface. In particular, the inhomogeneous distribution of Cu in the alloy microstructure (intentionally developed to optimize mechanical properties of the alloy) is known to be responsible for the low pitting resistance of the alloy.<sup>63,64</sup> In an attempt to address this question, energy-dispersive x-ray (EDX) analysis was performed on selected samples. Figures 13 and 14 show a typical result. Note in Figure 13 that (as observed previously in Figures 11 and 12) the oxidation was highly localized and resulted in a visible pit after coating removal. However, unlike the result of Figure 11 where the reduction reaction was confined largely to the defect area, the reduction process in Figure 13 was distributed rather uniformly across both the defect and the polymer.

Figure 14 shows scanning electron micrographs of the sample of Figure 13. Seven regions are labeled on the micrographs: A, B and C in the scribe area; D and E in defect-free regions; and F and G in the pit area. The copper content of each of these regions is reported in Table 1. The "mass effect" may render these analytical results semi-quantitative at best,<sup>65</sup> and the actual Cu content in the Cu rich regions may be higher than that reported in Table 1. It is clear from these results that the site where the pitting occurred is a Cu-rich site, containing well above the 4% to 5% average Cu content expected for this alloy.

While we cannot assign a specific phase to the Cu-rich regions F and G, the most common such phase for this alloy is reported to be the S phase particles ( $\text{Al}_2\text{CuMg}$ ), comprising approximately 60% of particles greater than 0.5 to 0.7  $\mu\text{m}$  and covering approximately 2.7% of the alloy surface.<sup>66</sup> Furthermore, S phase particles are active relative to the aluminum matrix phase and are reported to undergo partial dissolution by dealloying.<sup>66</sup> Such active regions are likely candidates for the site of oxidation observed in the SVET experiments. The Cu content of S phase particles is ca. 45% and increases as a result of dealloying.<sup>66</sup> Our observation of only ca. 20% Cu in regions F and G suggests that Cu is preferentially removed from these particles, perhaps a consequence of its ability to complex with the conducting polymer as noted above.

The second most abundant Cu rich phase in the alloy is  $\text{Al}_{24}\text{Cu}_2\text{FeMn}$ , comprising approximately 12.3% of all particles and covering approximately 0.85% of the surface.<sup>66</sup> These particles are among the largest found on the alloy surface<sup>66</sup> and contain ca. 14% Cu. The Cu contents observed in regions F and G are larger than this (20%), suggesting that if these particles were responsible for the observed oxidation process, then dealloying leading to an enrichment in Cu must have occurred. However, no Fe or Mn was detected in these regions, whereas some Mg was observed (though less than 1%). This supports the notion that the Cu rich regions are S phase particles.

**Poly(3-octyl pyrrole) Coating on Pure Al Metal.** If a Cu-rich phase(s) of the Al 2024-T3 alloy is responsible for the highly localized oxidation currents observed with POP-coated alloy, then a somewhat different result might be expected for experiments conducted on pure aluminum metal. Figure 15 shows current density maps for POP-coated Al (99.998%). As observed with the alloy, there was a significant time delay before the onset of any observable current, at which point only reduction was observed in the defect area. However, in contrast to the alloy where the oxidation current was always very localized, the oxidation current on pure Al appeared to be much more distributed across the substrate surface. In particular, the current appeared primarily around the perimeter of the exposed area, as distant from the defect as possible (Figure 15). When the coating was removed, no pitting was observed and no visible corrosion products remained on the Al surface. Instead, the surface was shiny, suggesting a rather uniform oxidation of the aluminum surface, most likely producing  $\text{Al}^{3+}$  ions that were incorporated into (or perhaps transported through) the coating. Further experiments are planned to elucidate the details of this process. Nevertheless, these observations support the notion that Cu rich regions in the alloy are responsible for the localized oxidation current observed with the POP-coated Al 2024-T3.

**Long Term Immersion Studies.** EIS was used to study samples that have been under immersion for approximately 600 days. EIS data were collected at the open circuit potential for increasing times of immersion. Dilute Harrison solution was chosen as the immersion electrolyte due to its ability to imitate an industrial atmospheric environment.

At this point in the study, the samples show relatively different responses to the stresses of constant immersion. It is possible to notice visual differences (Figure 16) amongst the Cr-epoxy/polyurethane, POP/polyurethane, and PODP/polyurethane

samples. It can be seen that the least change and greatest inhibition of blister development occurs in the POP/polyurethane sample. It must be reiterated here that the overall coating thickness of the Cr-Epoxy/polyurethane system is greater than that of our ECP/polyurethane systems. It is suggested that this diminished blister development is not due to greater barrier properties of the ECP/polyurethane systems. The ECPs do not act as a barrier coating. Rather, it is thought that they can aid in the transport of both electronic charge and ion movement.<sup>18</sup>

In addition to visual changes, electrochemical changes were evident by the impedance spectra shown in Figure 17. In Figure 17a, it can be seen that the Polyurethane/Cr-Epoxy/Al 2024-T3 sample had a high impedance at the start of immersion (greater than  $10^9$  Ohms). Although initially stable, the sample showed drastic failure at 358 days. At the time of failure rather large blisters, over 3 mm in diameter, were evident (Figure 16a). The rapid growth and/or rupture of this blister may be responsible for such a drastic drop in impedance. The Polyurethane/POP/Al 2024-T3 sample continued to maintain the initial impedance value (Figure 17b) and the Polyurethane/PODP/Al 2024-T3 sample started to show signs of failure, with the impedance decreasing at day 376 to a value of  $10^7$  (Figure 17c). The visual appearances of the samples shown in Figure 16 support the EIS results of Figure 17, with the sample exhibiting the smallest visual change (the polyurethane/POP/Al 2024-T3) also displaying the smallest decrease in impedance.

**Electrochemical Noise Method.** ENM is a useful tool in the studies of corrosion due to its non-perturbing behavior.  $R_n$  is calculated from the spontaneous fluctuations in current and voltage that arise between two nominally identical samples. In this study, the samples are non-scribed ECPs with no polyurethane topcoat. In Figure 18a, a plot of  $R_n$  vs. immersion time for the POP sample is shown. The values of  $R_n$  remained between  $10^4$  and  $10^5 \Omega$  throughout the immersion period. In Figure 18b, a plot of  $R_n$  Vs. immersion time for the PODP sample is shown. While PODP also had value of  $R_n$  between  $10^4$  and  $10^5 \Omega$ , it does appear it is very unstable, having large fluctuations when compared to the relatively stable  $R_n$  of POP. It is possible to notice cyclic fluctuations that occur during the first few days in the insets provided in Figures 18a and 18b. Fluctuations in  $R_n$  have been reported elsewhere by this laboratory.<sup>18</sup> This cyclic behavior is markedly different from the behavior experienced with barrier coatings. Barrier coatings generally show a continually decreasing  $R_n$  with immersion time. Films that have good barrier properties generally have high  $R_n$  values, well above  $10^7 \Omega$ . Films with poor barrier properties have corresponding low  $R_n$  values, around or below  $10^5 \Omega$ . The relationship between  $R_n$  and barrier properties of coatings has been discussed elsewhere.<sup>67</sup> It was fully expected that a low  $R_n$  value would be seen for the ECP samples. It was never assumed that a material that allows both electronic and ionic conduction would provide barrier protection.

Perhaps the differences found between the PODP and POP system are dependent on the stability of adherent oxide layer. It is suggested that a less adherent oxide layer would fail and subsequently reform, giving rise to large fluctuations in  $R_n$ . The POP system may allow for the formation of an extremely stable, tightly adhering oxide layer,

thus providing better protection to the underlying substrate. With a stable oxide layer present, less fluctuation would be noticed.

**Polarization Scans.** Polarization scans allow the rate of corrosion to be determined. The anodic branch can relate to the oxidation of the metal or the ECP. The cathodic branch can be due to numerous reduction reactions. Common reduction reactions are the reduction of  $O_2$  or  $H^+$ . Surprisingly, the results for PODP and POP samples varied greatly. While the POP appears to passivate the scribe, as shown by the increase (less negative) in the  $E_{corr}$ , the corrosion potential for the PODP sample continues to get more negative (Figures 19a and 19b). This would correspond to a more active system, perhaps due to the failure of the adherent oxide layer.

**pH Changes During Immersion in DHS.** The pH changes of the immersion electrolyte solution were monitored during the ENM experiments. It can be seen (Figure 20) that the general trend is an increase in pH during immersion time. It is interesting to note that the increase in pH found in this present study is in direct opposition of the results reported for polyaniline.<sup>18</sup> It is proposed that the increase in pH seen in this study is due to aluminum hydroxide that is the corrosion product of the aluminum alloy 2024-T3. Aluminum hydroxide is slightly soluble in water, and thus increases the pH of the immersion solution. The decrease in pH for polyaniline reported elsewhere is attributed to the dedoping of the polyaniline, thus releasing  $H^+$  into the immersion electrolyte.

**Preliminary Scribed Prohesion Results.** Scribed samples have recently been placed in Prohesion cyclic exposure. EIS experiments were completed in an area void of defects, i.e. not at the scribe defect. Although only initial results are available at this time, they do provide a better understanding of the usefulness of ECPs as corrosion inhibitors. It is very interesting to note that while the Polyurethane/Cr-Epoxy/Al 2024-T3 system shows an initial decrease in impedance after 117 hours of Prohesion exposure, the PODP system is able to maintain the initial impedance value (Figures 21a-c). Even more promising is the POP system. After 117 hours of Prohesion exposure, the POP system actually shows an increase in impedance. This increase may be due to a growth in the adherent oxide layer. Although these results are purely preliminary, the experiment will be continued until failure of the systems. Currently no visual changes were noticeable at the scribe or elsewhere on the sample surface. Complete results will be reported at a later date.

## CONCLUSIONS

The chromated-epoxy coating delayed the onset of corrosion of both the steel and aluminum substrates compared to a plain epoxy coating. Apparently the chromated-epoxy coating initially promoted formation and/or stabilization of a passive layer within the defect region, slowing the corrosion process. However, the aggressive immersion conditions eventually led to a breach of this passive layer and corrosion current began to flow. Once detectable corrosion commenced, the chromated-epoxy coating actually appeared to sustain the current at both metals for a longer period of time than observed with the plain epoxy coating. This surprising observation may be an important aspect of

the long-term protection mechanism of chromate-based coatings, leading to passive films of different composition and perhaps more resilience than that produced in the absence of chromate.

Poly(3-octyl pyrrole) and poly(3-octadecyl pyrrole) have the ability to inhibit corrosion, with poly(3-octyl pyrrole) showing greater inhibition. In this regard, the POP and PODP coatings are similar to chromated-epoxy coatings. However the POP coatings produce even longer delays before the onset of current flow in and around the defect. The defect apparently is protected by a mechanism involving formulation and/or stabilization of a passive layer in the defect, likely a consequence of the ability of these coatings to render the surface potential within the defect more positive (noble). Eventually, however, the aggressive immersion medium breaches the passive layer and corrosion commences. At this point, the behaviors of steel and of aluminum differ.

Further investigations will be carried out to clarify and verify the protection offered by the ECPs.

#### **ACKNOWLEDGMENTS**

This work was supported by the Air Force Office of Scientific Research, Grant Nos. F49620-96-1-0284 and F49620-97-1-0376 (AASERT), North Dakota State University. We are grateful to Dr. Chee O. Too and Dr. Syed A. Ashraf of the Intelligent Polymer Research Institute (University of Wollongong, Australia) for synthesis of the poly(3-octyl pyrrole) used in this work.

## REFERENCES

1. S.M. Cohen, *Corrosion*, **51**, 71 (1995).
2. W-K. Lu, S. Basak, and R.L. Elsenbaumer, *Handbook of Conducting Polymers*, 2<sup>nd</sup> Ed., T.a. Skotheim, R.L. Elsenbaumer, J.R. Reynolds, Eds., New York, NY (1998) p. 881.
3. D.W. Deberry, *J. Electrochem. Soc.*, **132**, 1022 (1985).
4. W.K. Lu, R.L. Elsenbaumer, B. Wessling, *Synth. Met.*, **71**, 2163 (1995).
5. N. Ahmad, A.G. MacDiarmid, *Synth. Met.*, **78**, 103 (1996).
6. K. G. Thompson, C.J. Bryan, B.C. Benicewicz, D.A. Wroblewski, *ACS Polymer Preprints*, **35**, 265 (1994).
7. M. Fahlman, S. Jasty, A.J. Epstein, *Synth. Met.*, **85**, 1323 (1997).
8. J.R. Santos, Jr., L.H.C. Mattoso, A.J. Motheo, *Electrochimica Acta*, **43**, 308 (1998).
9. A. Talo, O. Forsén, and S. Yläsaari, *Synthetic Metals*, **102**, 1394 (1999).
10. B. Wessling and J. Posdorfer, *Synthetic Metals*, **102**, 1400 (1999).
11. M-C. Bernard, A. Hugot-LeGoff, S. Joiret, N. N. Dinh, and N. N. Toan, *Synthetic Metals*, **102**, 1383 (1999).
12. M-C. Bernard, C. Deslouis, T. El Moustafid, A. Hugot-LeGoff, S. Joiret, and B. Tribollet, *Synthetic Metals*, **102**, 1381 (1999).
13. Kulszewicz-Bajer, M. Zagórska, A. Bany, and L. Kwiatkowski, *Synthetic Metals*, **102**, 1385 (1999).
14. D. E. Tallman, Y. Pae, G. P. Bierwagen, *Corrosion*, **55**, 779 (1999).
15. R.J. Racicot, R.L. Clark, H-B. Liu, S.C. Yang, M.N. Alias, R. Brown, *Proc. SPIE-Int. Soc. Opt. Eng.*, **2528**, 251 (1995).
16. R.J. Racicot, R.L. Clark, H-B. Liu, S.C. Yang, M.N. Alias, R. Brown, *Mater. Res. Soc. Symp. Proc.*, **413**, 529 (1996).
17. J. Epstein, J. A. O. Smallfield, H. Guan, and M. Fahlman, *Synthetic Metals*, **102**, 1374 (1999).
18. D. E. Tallman, Y. Pae, G. P. Bierwagen, *Corrosion*, (1999) submitted.
19. R.J. Racicot, S.C. Yang, R. Brown, *Corrosion*, **531**, 1 (1997).
20. F. Beck and R. Michaelis, *J. Coating Tech.*, **64**, 59 (1992).
21. Ferreira, S. Aeiyach, J. J. Aaron, P. C. Lacaze, *Electrochim. Acta*, **41**, 1801 (1996).
22. N. V. Krstajic, B. N. Grgur, S. M. Jovanovic, and M. V. Vojnovic, *Electrochim. Acta*, **42**, 1685 (1997).
23. B. N. Grgur, N. V. Krstajic, M. V. Vojnovic, C. Lacnjavac, and Lj. Gajic-Krstajic, *Progress in Organic Coatings*, **33**, 1 (1998).
24. J. Reut, A. Öpik, and K. Idla, *Synthetic Metals*, **102**, 1392 (1999).

25. C. A. Ferreira, S. Aeiyach, A. Coulaud, and P. C. Lacaze, *Journal of Applied Electrochemistry*, **29**, 259 (1999).
26. J. Y. Lee, D. Y. Kim, and C. Y. Kim, *Synthetic Metals*, **74**, 103 (1995).
27. S. A. Ashraf, F. Chen, C. O. Too, and G. G. Wallace, *Polymer*, **37**, 2811 (1996).
28. G.P. Bierwagen, *J.Electrochem. Soc.*, (1994) L141.
29. H. S. Isaacs and B. Vyas, in *Electrochemical Corrosion Testing*, ASTM STP- 727, F. Mansfield and U. Bertocci, Editors, American Society for Testing and Materials, pp. 3-31, Philadelphia, PA (1981).
30. D. A. Sargeant, *Corrosion Prevention and Control*, **44**, 91 (1997).
31. I. Sekine, M. Yuasa, K. Tanaka, T. Tsutsumi, F. Koizumi, N. Oda, H. Tanabe, and M. Nagai, *Shikizai*, **67**, 424 (1994).
32. I. Sekine, *Progress in Organic Coatings*, **31**, 73 (1997).
33. R. S. Lillard, P. J. Moran, and H. S. Isaacs, *J. Electrochem. Soc.*, **139**, 1007 (1992).
34. M. W. Wittmann and S. R. Taylor, *Advances in Corrosion Protection by Organic Coatings II*, D. Scantlebury and M. Kendig, Editors, PV 95-13, p. 158, The Electrochemical Society Proceedings Series, Pennington, NJ (1995).
35. R. B. Leggat and S. R. Taylor, *Corrosion*, **55**, 984 (1999).
36. E. Bayet, F. Huet, M. Keddam, K. Ogle, and H. Takenouti, *J. Electrochem. Soc.*, **144**, L87 (1997).
37. E. Bayet, F. Huet, and H. Takenouti, *Electrochimica Acta*, **44**, 4177 (1999).
38. P. J. Kinlen, V. Menon, and Y. Ding, *J. Electrochem. Soc.*, **146**, 3690 (1999).
39. H. N. Rosen and J. W. Martin, *Journal of Coatings Technology*, **63**, 85 (1991).
40. C. R. Hegedus, D. F. Pulley, S. J. Spadafora, A. T. Eng, and D. J. Hiest, *J. Coatings Technology*, **61**, 31 (1989).
41. R. S. Fishman, D. A. Kurtz and G. P. Bierwagen, *Progress in Organic Coatings*, **21**, 387 (1993).
42. W. H. Smyrt and M. Lien, *Applications of Electroactive Polymers*, B. Scrosati, Editor, p. 29, Chapman and Hall, UK (1993).
43. D. A. Jones, *Principles and Prevention of Corrosion*, 2nd Edition, p. 490, Prentice Hall, Upper Saddle River, NJ (1996).
44. Z. W. Wicks, Jr., F. N. Jones and S. P. Pappas, *Organic Coatings: Science and Technology*, 2nd Edition, pp. 131-133, Wiley-Interscience, New York (1999).
45. P. J. Kinlen, D. C. Silverman, and C. R. Jeffreys, *Synthetic Metals*, **85**, 1327 (1997).
46. J. He, V. J. Gelling, D. E. Tallman, G. P. Bierwagen, G. G. Wallace, *J. Electrochem. Soc.*, **47**, 3667 (2000).
47. M. Zin, R. L. Howard, S. J. Badger, J. D. Scantlebury, and S. B. Lyon, *Progress in Organic Coatings*, **33**, 203 (1998).

48. K. C. Tsai and C. H. Tsai, in *Proc. 4th Asian-Pacific Conference*, Materials Conservation and Corrosion Control, Vol. 1, p. 491, Tokyo, May 26-31, 1985.
49. H. Wienand and W. Ostertag, *Modern Paint and Coatings*, November 1984, pp. 38-48.
50. G. Adrian and A. Bittner, *J. Coatings Technology*, **58**, 59 (1986).
51. J. R. Waldrop and M. W. Kendig, *J. Electrochem. Soc.*, **145**, 1 (1998).
52. Z. Szklarska-Smialowska and R. W. Staehle, *J. Electrochem. Soc.*, **121**, (1974) 1146.
53. J. Sinko, *Progress in Organic Coatings*, in press (2000).
54. M. W. Kendig, A. J. Davenport and H. S. Issacs, *Corrosion Science*, **34**, 41 (1993).
55. G. B. Hatch, Influence of Inhibitors on Differential Aeration Attack on Steel. II- Dichromate and Orthophosphate, NACE National Conference, NACE, Houston (1964).
56. J. Zhao, G. Frankel and R. McCreery, *J. Electrochem. Soc.*, **145**, 2258 (1998).
57. B. P. Boffardi, in *Reviews on Corrosion Inhibitor Science and Technology*, A. Raman and P. Labine (eds.), NACE, Houston (1993).
58. I. J. Buerge and S. J. Hug, *Environmental Science and Technology*, **31**, 5 (1997).
59. L. Xia and R. L. McCreery, *J. Electrochem. Soc.*, **145**, 3083 (1998).
60. J. He, V. J. Gelling, D. E. Tallman, G. P. Bierwagen, *J. Electrochem. Soc.*, **47**, 3661 (2000).
61. M. B. Inoue, K. W. Nebesny, Q. Fernando, Ma. M. Castillo-Ortega and M. Inoue, *Synthetic Metals*, **38**, 205 (1990).
62. A. Deronzier and J-C. Moutet, *Coordination Chemistry Reviews*, **147**, 339 (1996).
63. A. Gamer and D. Tromans, *Corrosion*, **35**, 55 (1979).
64. G. S. Chen, M. Gao and R. P. Wei, *Corrosion Science*, **52**, 8 (1996).
65. J. I. Goldstein, D. E. Newbury, P. Echlin, D. C. Joy, and E. Lifshin, *Scanning Electron Microscopy and X-Ray Microanalysis*, p. 339, plenum Press, New York (1981).
66. R. G. Buchheit, R. P. Grant, P. H. Hlava, B. McKenzie and G. L. Zender, *J. Electrochem. Soc.*, **144**, 2621 (1997).
67. G.P. Bierwagen, C. Jeffcoate, D.J. Mills, J. Li, S. Balbyshev, D.E. Tallman, *Prog. Org. Coat.*, **29** (1996) 21.

## FIGURE CAPTIONS

- Figure 1. Structure of Poly(3-alkyl pyrrole)
- Figure 2. Current density maps for the plain epoxy primer on steel at 5-minutes immersion in 3% NaCl. Top: three-dimensional representation of the z-component of the current density. Bottom: optical micrograph of the sample with current density vectors superimposed.
- Figure 3. Current density maps for plain epoxy primer on steel at 192-minutes immersion in 3% NaCl. Top: three-dimensional representation of the z-component of the current density. Bottom: optical micrograph of the sample (current density vectors omitted for clarity). Corrosion product is visible over much of the defect area.
- Figure 4. Current density maps for chromated-epoxy primer on steel at 169-minutes immersion in 3% NaCl. Top: three-dimensional representation of the z-component of the current density. Bottom: optical micrograph of the sample with current density vectors superimposed.
- Figure 5. Current density maps for chromated-epoxy primer on Al 2024-T3 alloy at 5-minutes (top) and 5.5-hours (bottom) immersion in dilute Harrison solution (three-dimensional representation of the z-component of the current density). See Figure 5 for the optical micrograph of this sample.
- Figure 6. Current density maps for chromated-epoxy primer on Al 2024-T3 alloy at 17.5-hours immersion in dilute Harrison solution. Top: three-dimensional representation of the z-component of the current density. Bottom: optical micrograph of the sample with current density vectors superimposed.
- Figure 7. Current density maps for POP on steel immersed in 3% NaCl (three-dimensional representation of the z-component of the current density). Top: at 5-minutes immersion. Bottom: at 2-hours and 46-minutes immersion. The optical micrograph of this sample is shown in Figure 2.
- Figure 8. Current density maps for POP on steel after 5-hours and 35-minutes immersion in 3% NaCl. Top: three-dimensional representation of the z-component of the current density. Bottom: optical micrograph of the sample with current density vectors superimposed.
- Figure 9. Current density map and optical micrograph for POP on Al 2024-T3 immersed in dilute Harrison solution. Top: three-dimensional representation of the z-component of the current density at 5-minutes immersion. Bottom: optical micrograph of sample with current vectors omitted for clarity.

- Figure 10. Current density maps for POP on Al 2024-T3 immersed in dilute Harrison solution (three-dimensional representation of the z-component of the current density). Top: at 22-hours and 14-minutes immersion. Bottom: at 23-hours and 14-minutes immersion.
- Figure 11. Current density maps for POP on Al 2024-T3 immersed in dilute Harrison solution. Top: three-dimensional representation of the z-component of the current density at 26-hours and 34-minutes immersion. Bottom: optical micrograph of sample with current density vectors superimposed.
- Figure 12. Optical micrograph of the sample from Figure 5 after removal of the POP coating, showing the region of undercoating pitting corrosion.
- Figure 13. Current density map for POP on Al 2024-T3 immersed in dilute Harrison solution (top) and optical micrograph of the sample after removal of the POP coating (bottom).
- Figure 14. Scanning electron micrograph of the sample of Figure 7 after removal of the POP coating showing the entire scan region (right; bar = 1 mm) and a magnified view of the pit region (left; bar = 100  $\mu\text{m}$ ). The letters denote regions of EDX analysis (see Table 1).
- Figure 15. Current density maps for POP on pure (99.998%) Al metal immersed in dilute Harrison solution at 8.6 hours immersion (top) and at 12.6 hours immersion (bottom).
- Figure 16. Optical Micrographs of Coating systems a) Polyurethane/Cr-Epoxy/Al 2024-T3 b) Polyurethane POP/Al 2024-T3 and c) Polyurethane/PODP/Al 2024-T3
- Figure 17. EIS spectra of Coating systems a) Polyurethane/Cr-Epoxy/Al 2024-T3 b) Polyurethane POP/Al 2024-T3 and c) Polyurethane/PODP/Al 2024-T3
- Figure 18.  $R_n$  versus immersion time for samples a) POP/Al 2024-T3 and b) PODP/Al 2024-T3
- Figure 19. Polarization scan curves for scribed coating systems a) POP/Al 2024-T3 and b) PODP/Al 2024-T3
- Figure 20. Change in pH of immersion electrolyte solution, Dilute Harrison Solution, as a function of immersion time of unscribed, no polyurethane topcoat samples.
- Figure 21. EIS spectra of Coating systems exposed to Prohesion Chamber  
a) Polyurethane/Cr-Epoxy/Al 2024-T3 b) Polyurethane POP/Al 2024-T3  
and c) Polyurethane/PODP/Al 2024-T3

Table 1. Copper content in designated regions of Figure 14.

Region	A	B	C	D	E	F	G
Cu (wt.%)	5.6	8.5	11.2	4.0	5.2	20.5	20.7

## Poly(3-alkyl pyrrole)

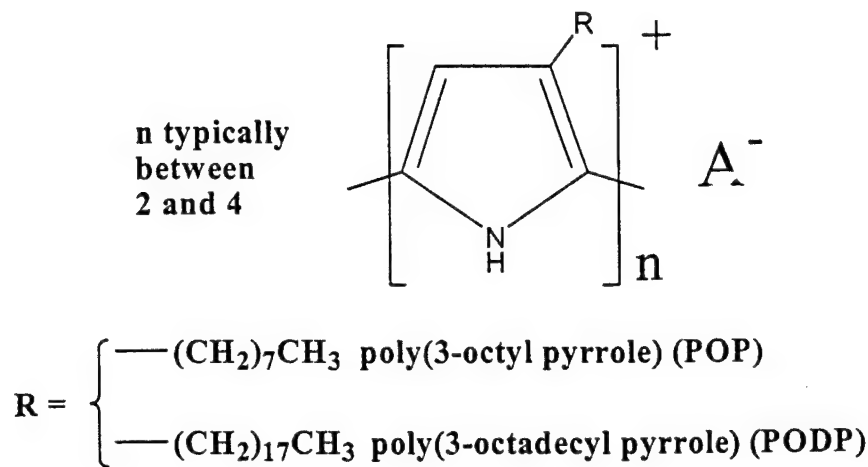
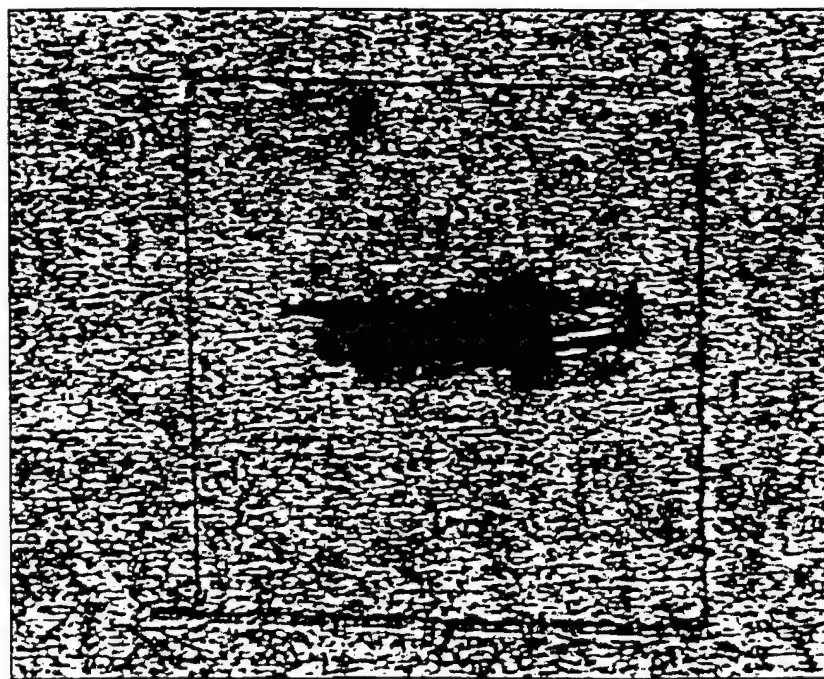
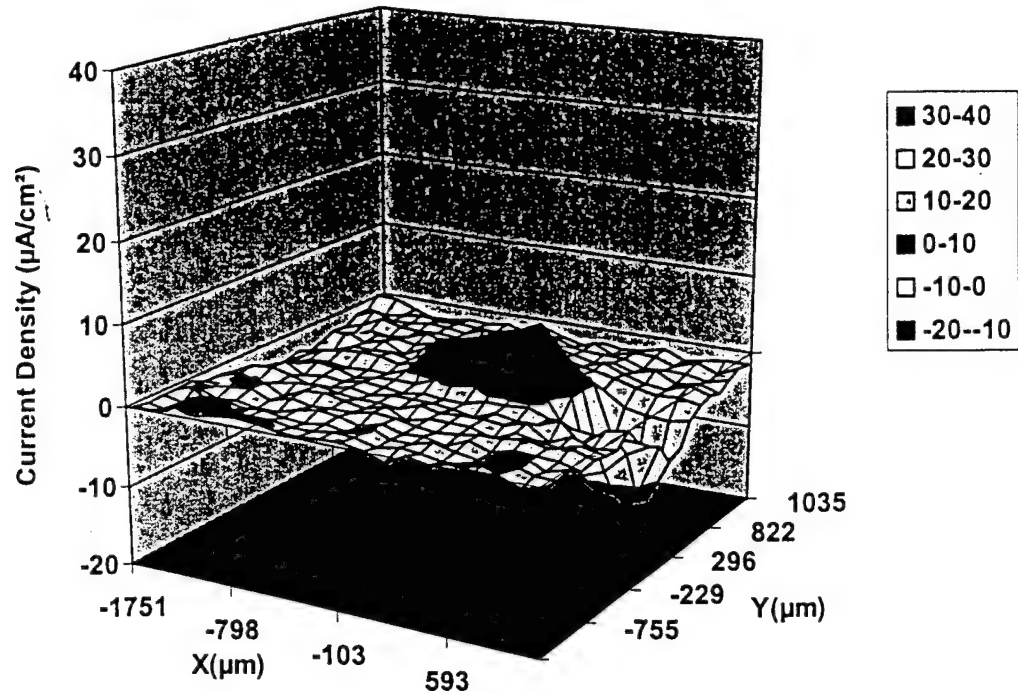
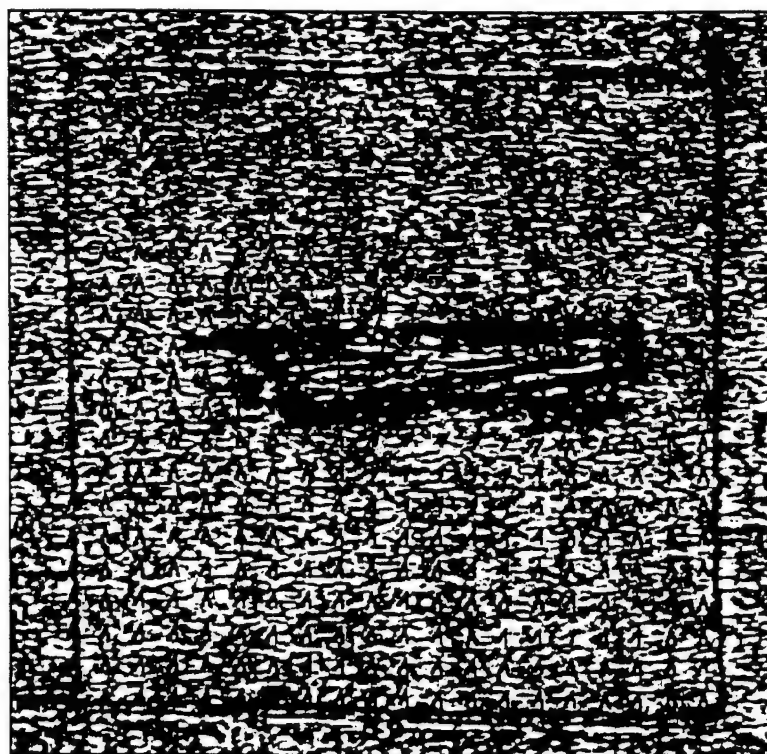
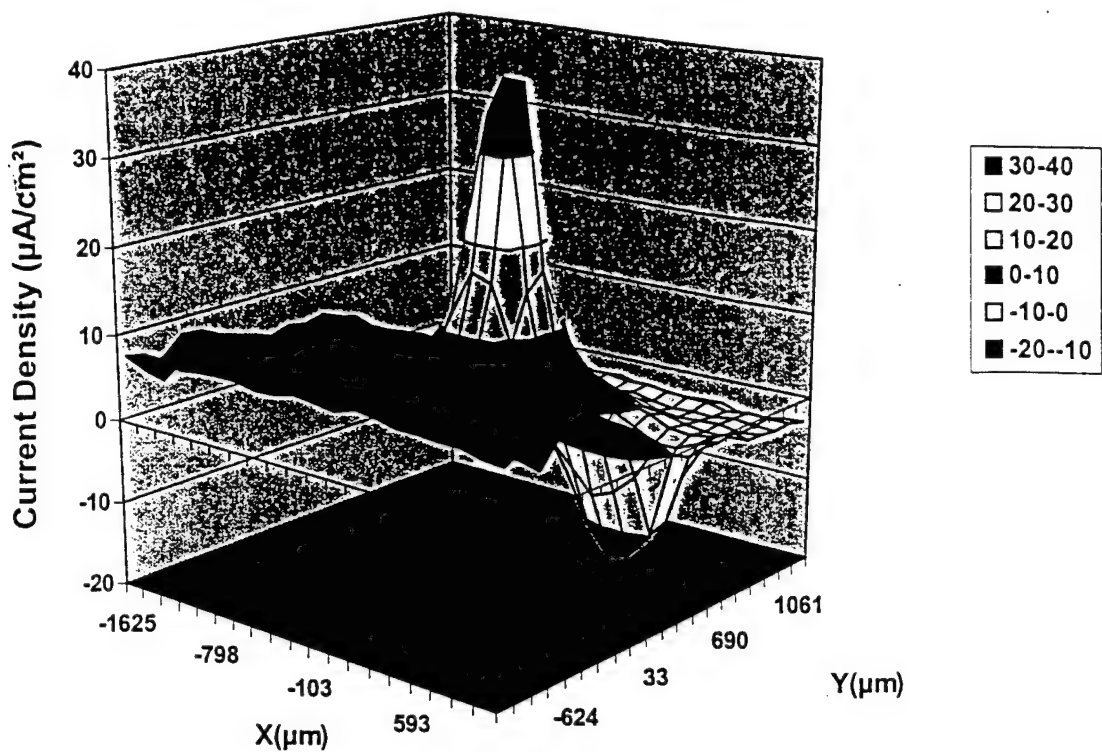


Figure 1



**Figure 2**



**Figure 3**

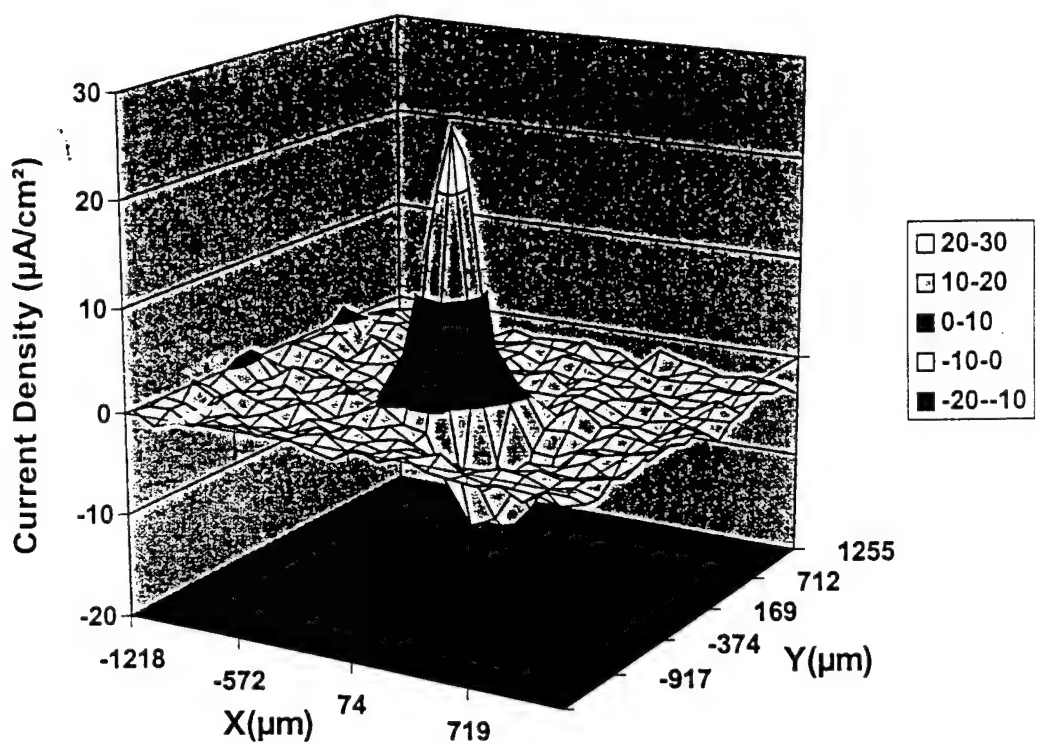


Figure 4

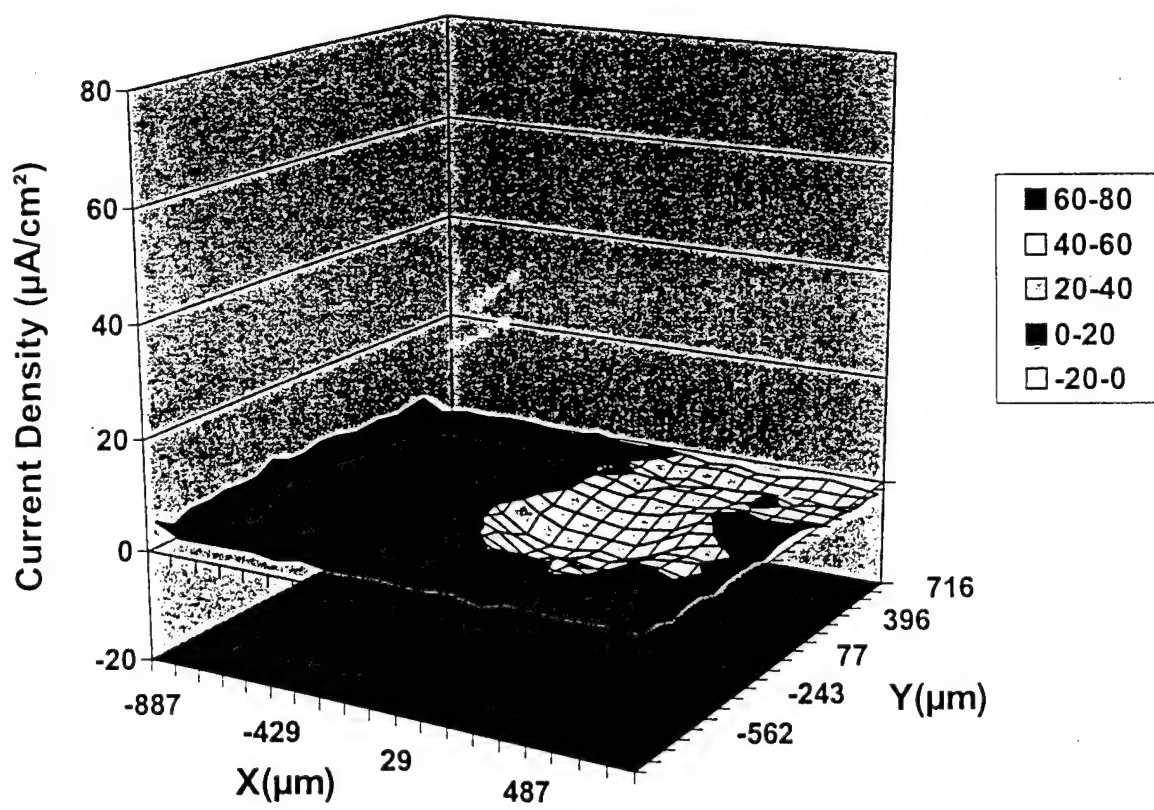
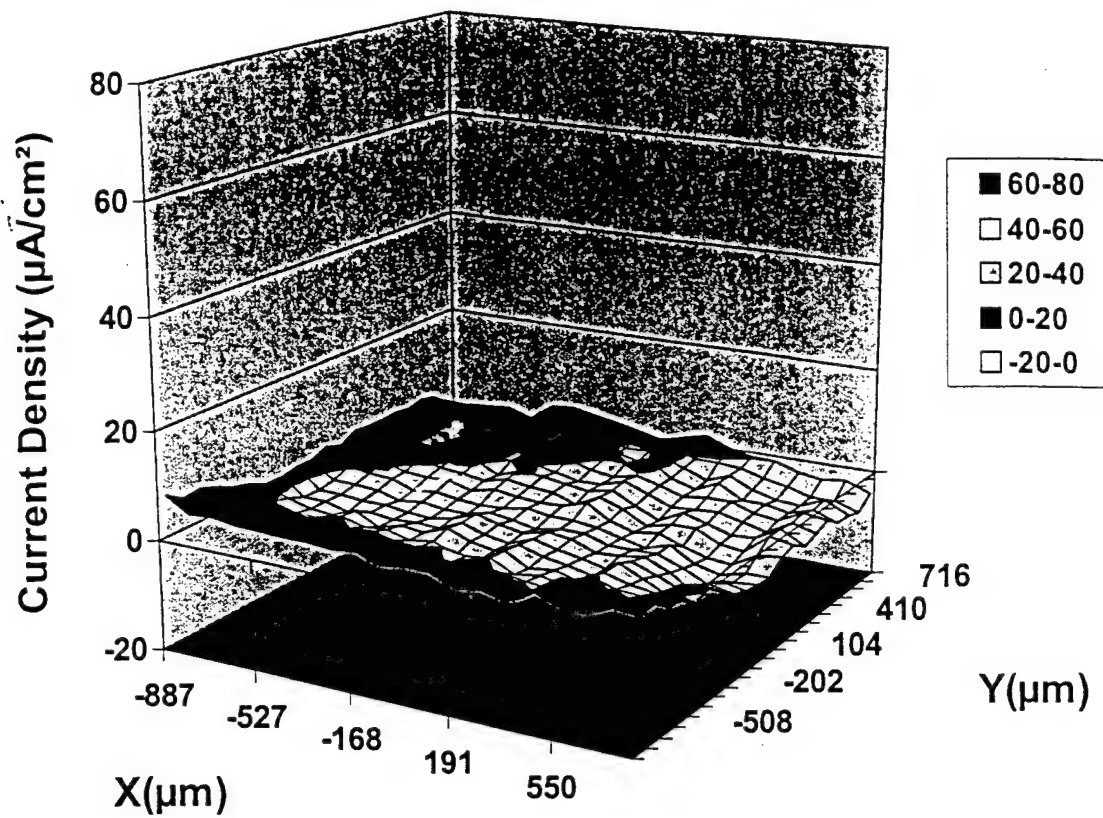


Figure 5

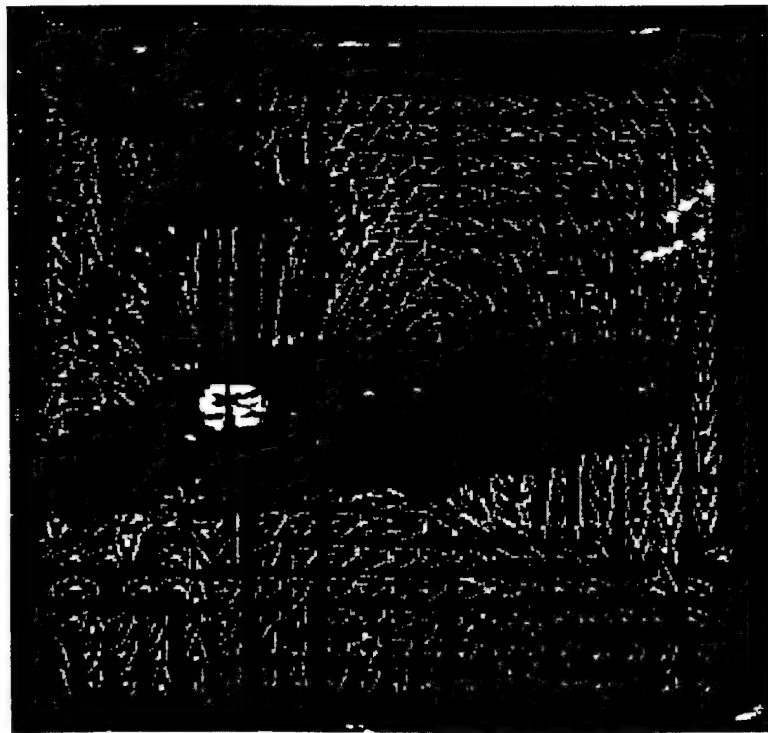
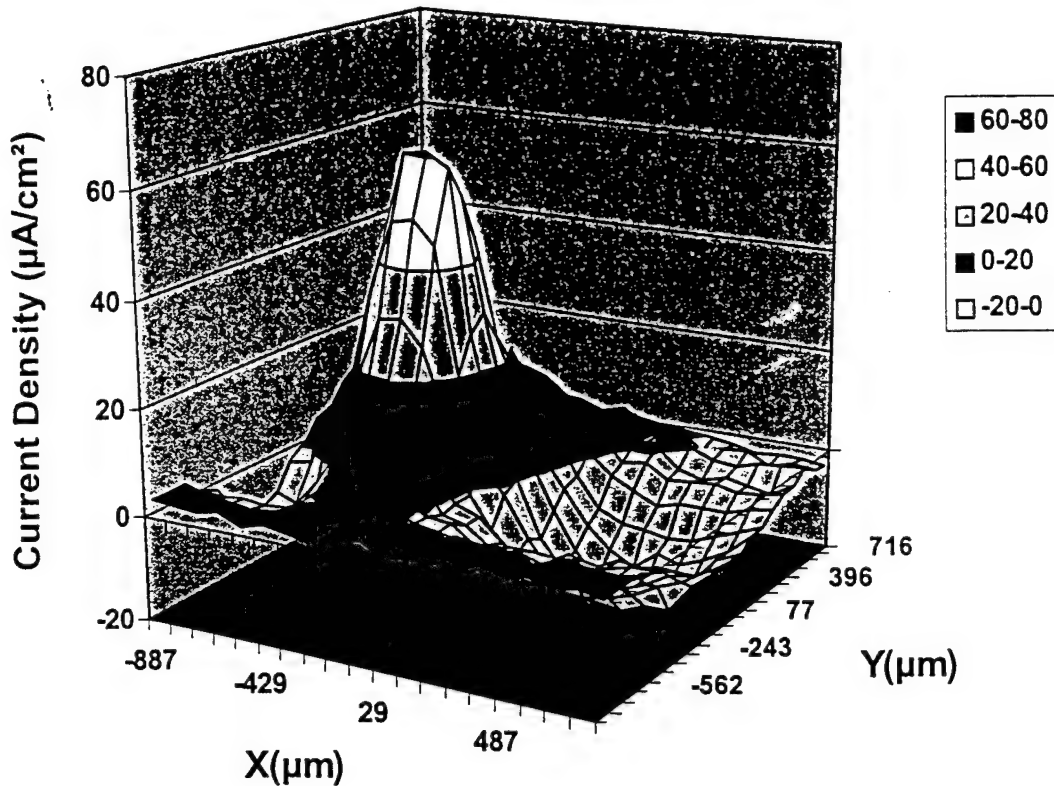
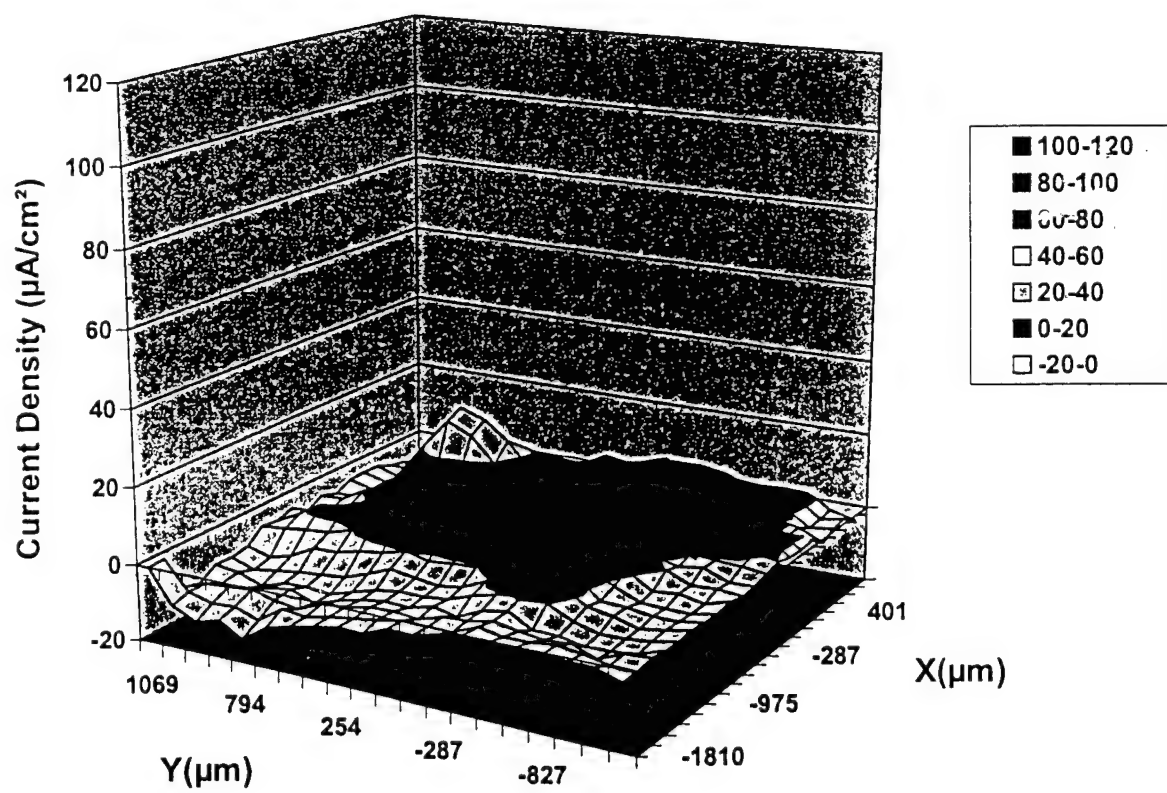
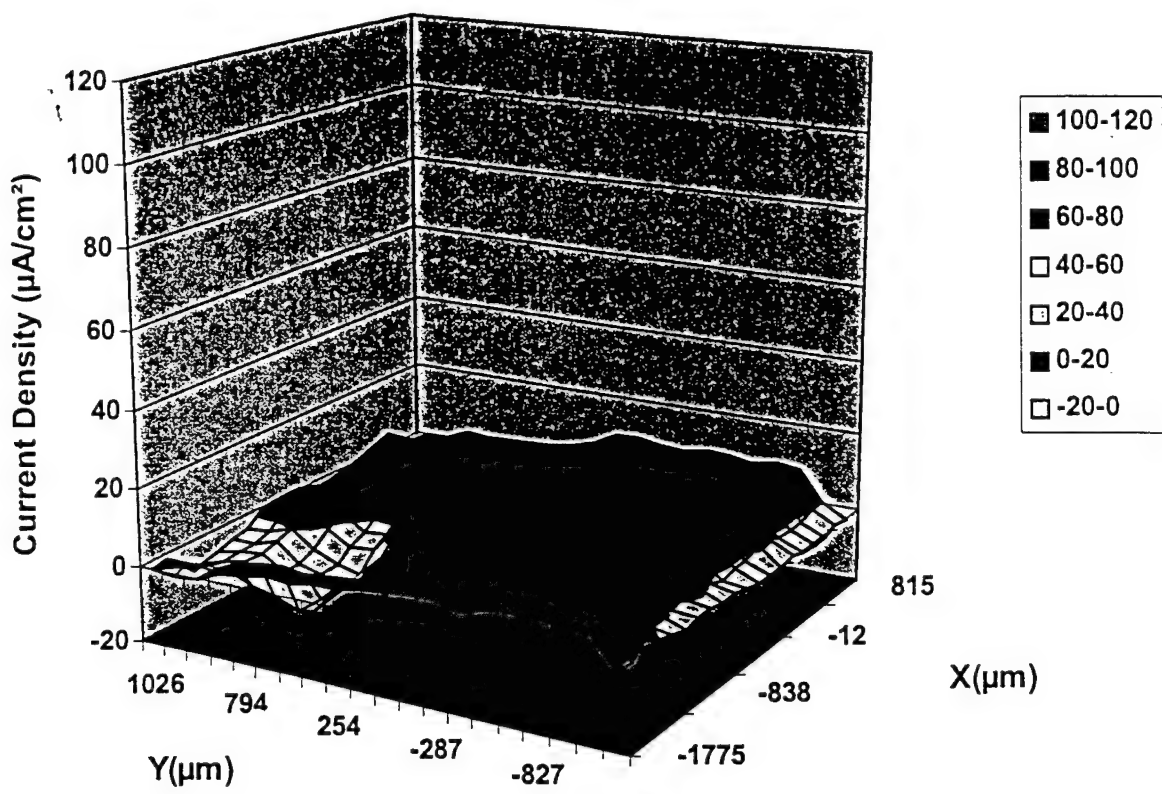


Figure 6



**Figure 7**

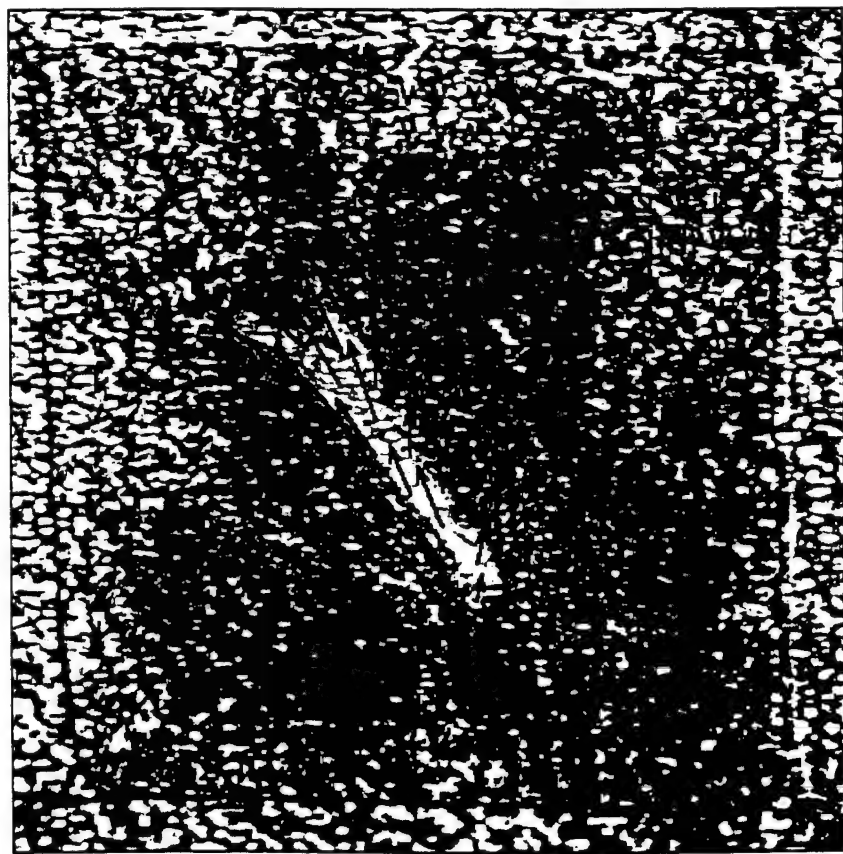
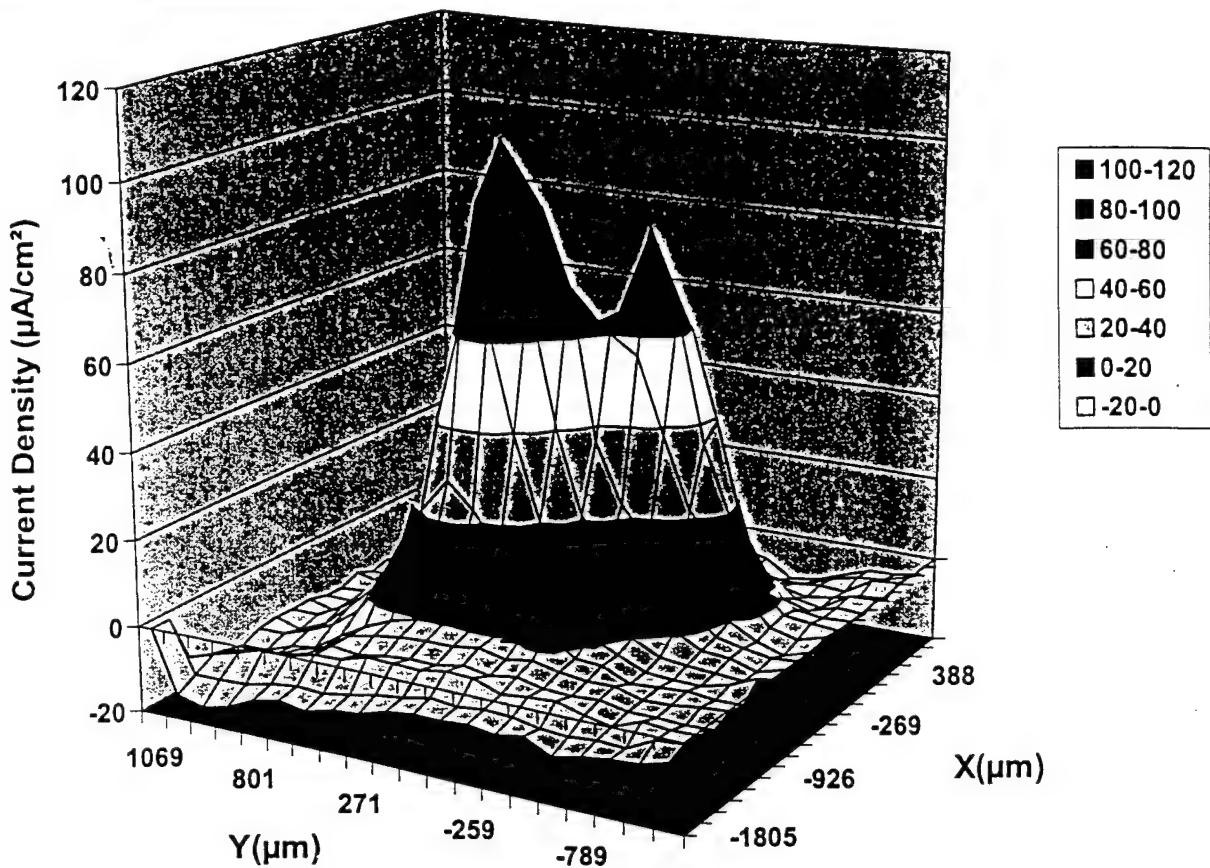


Figure 8

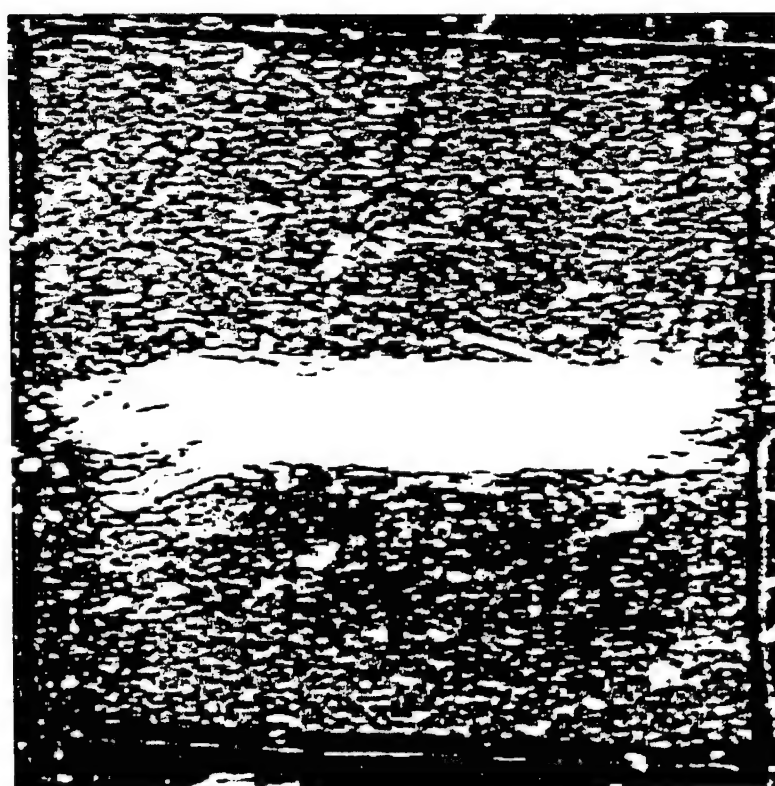
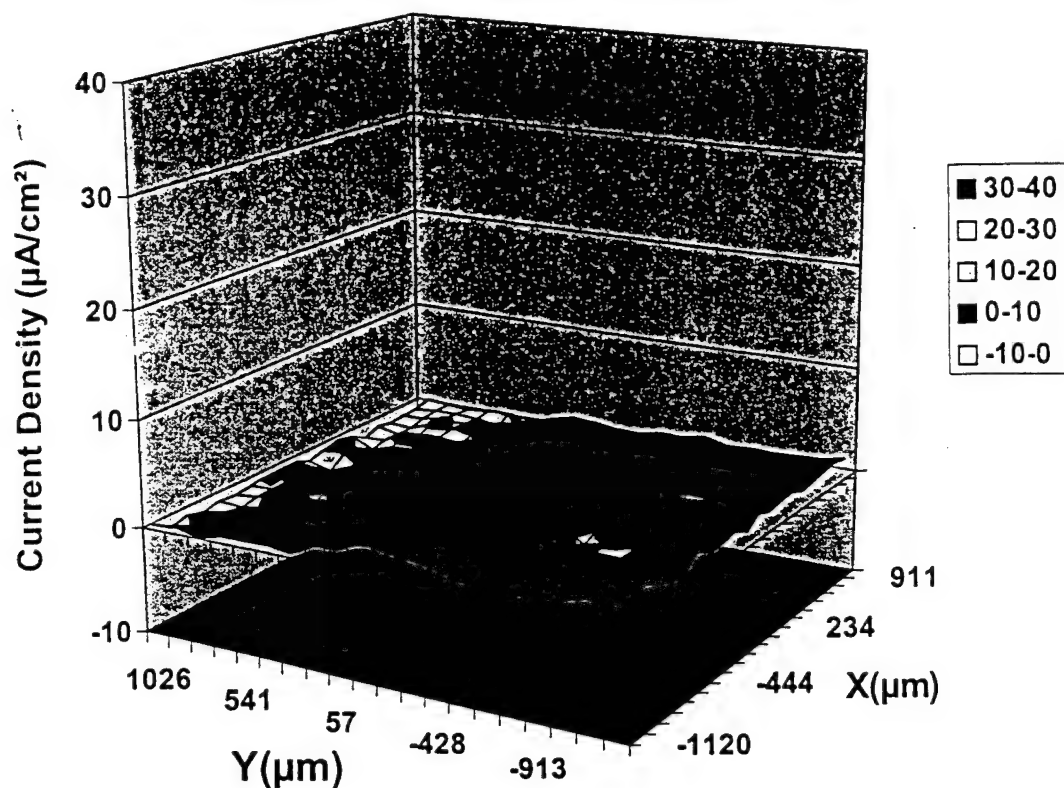
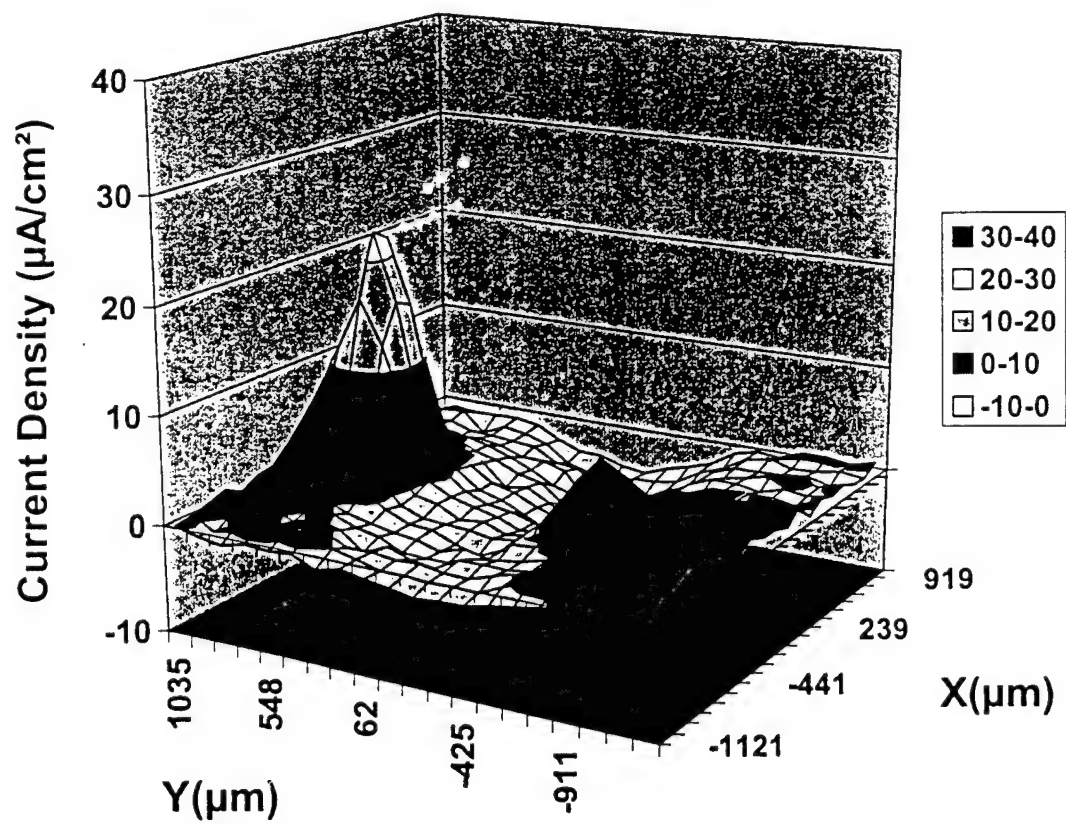
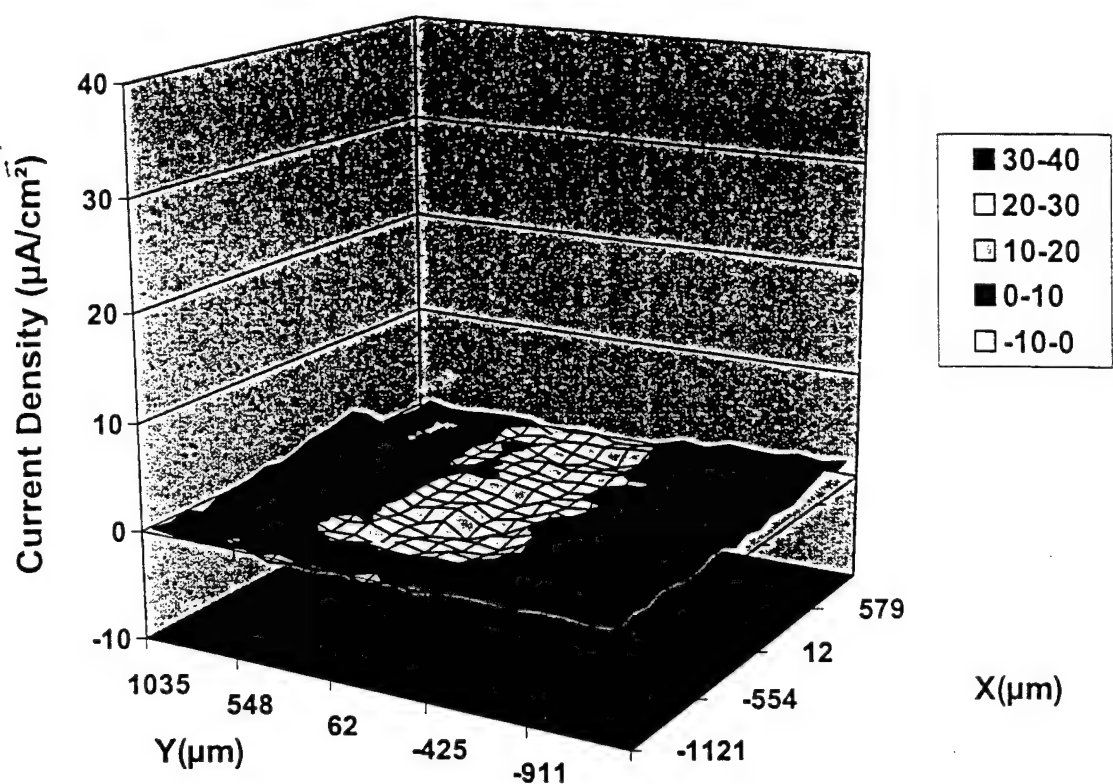


Figure 9



**Figure 10**

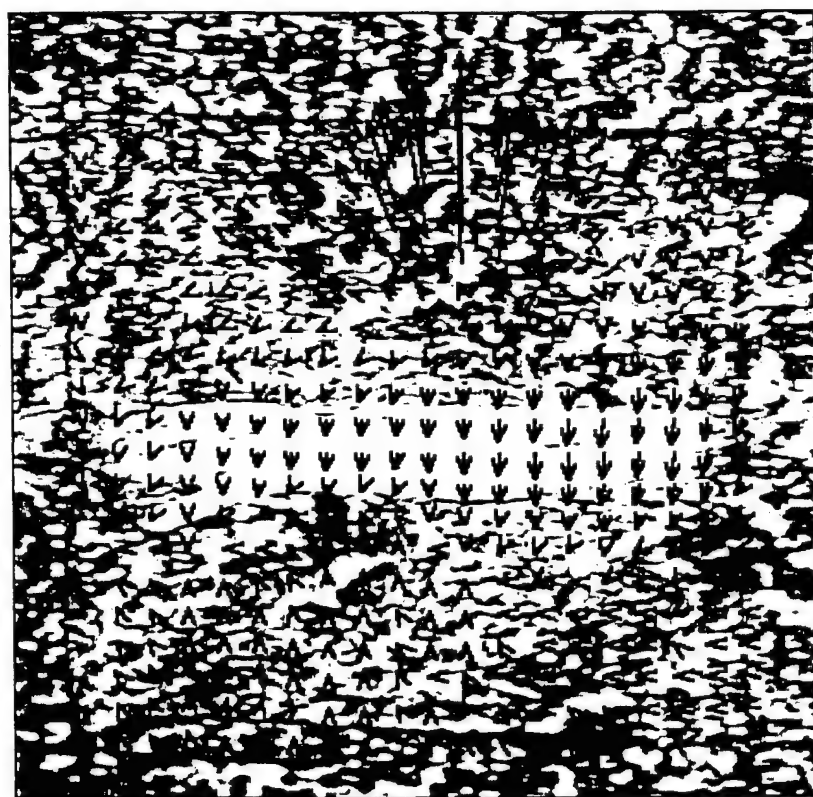
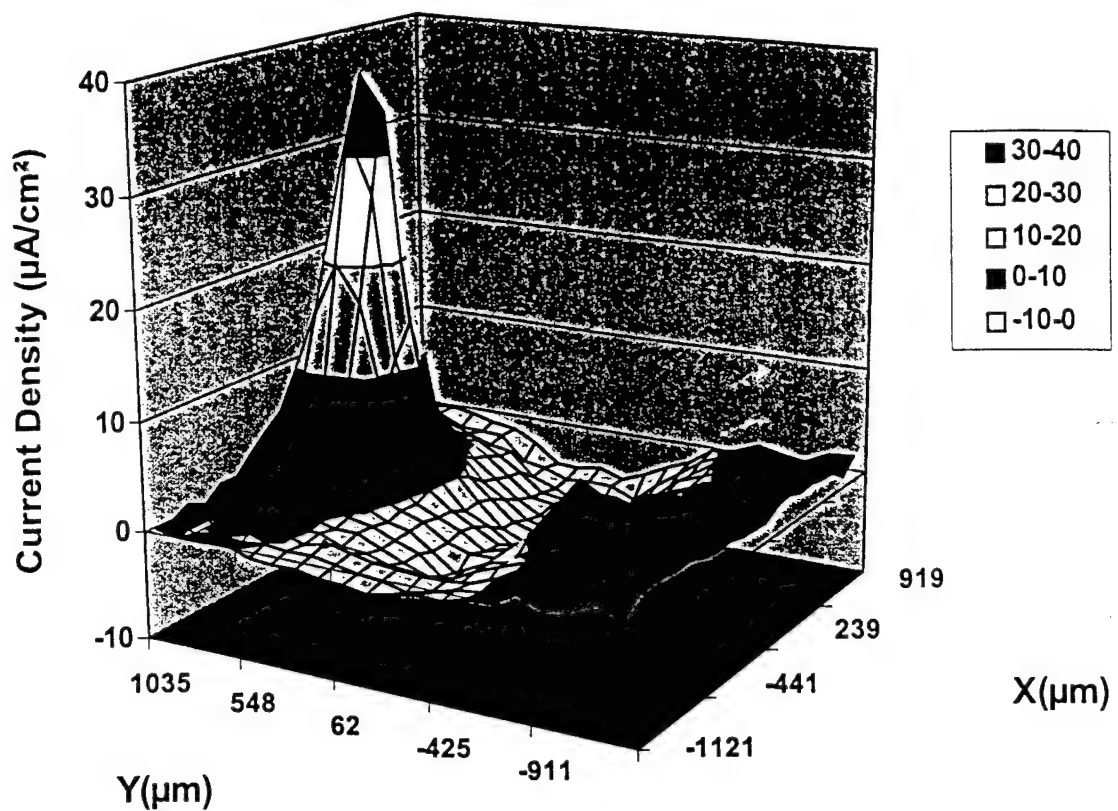


Figure 11

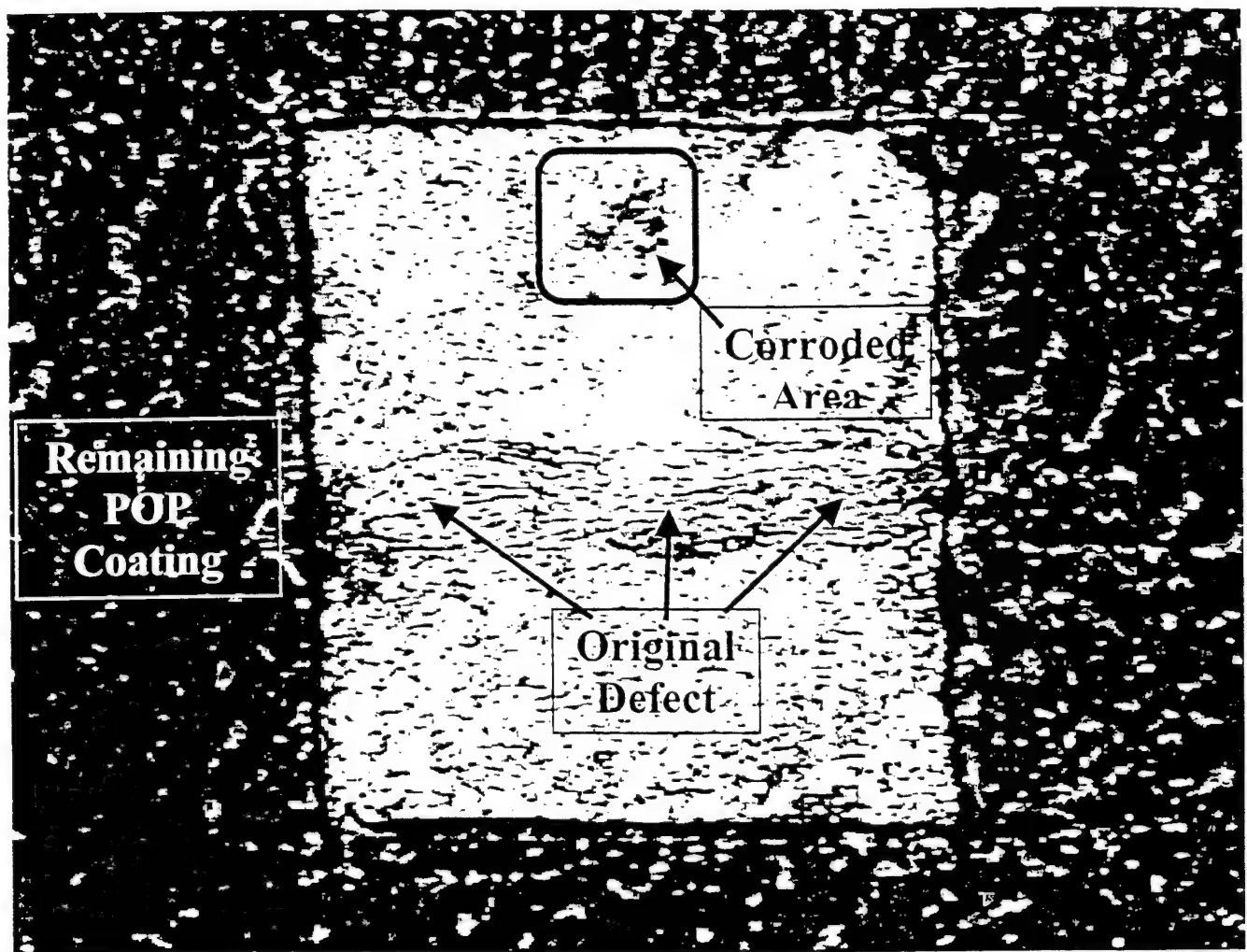
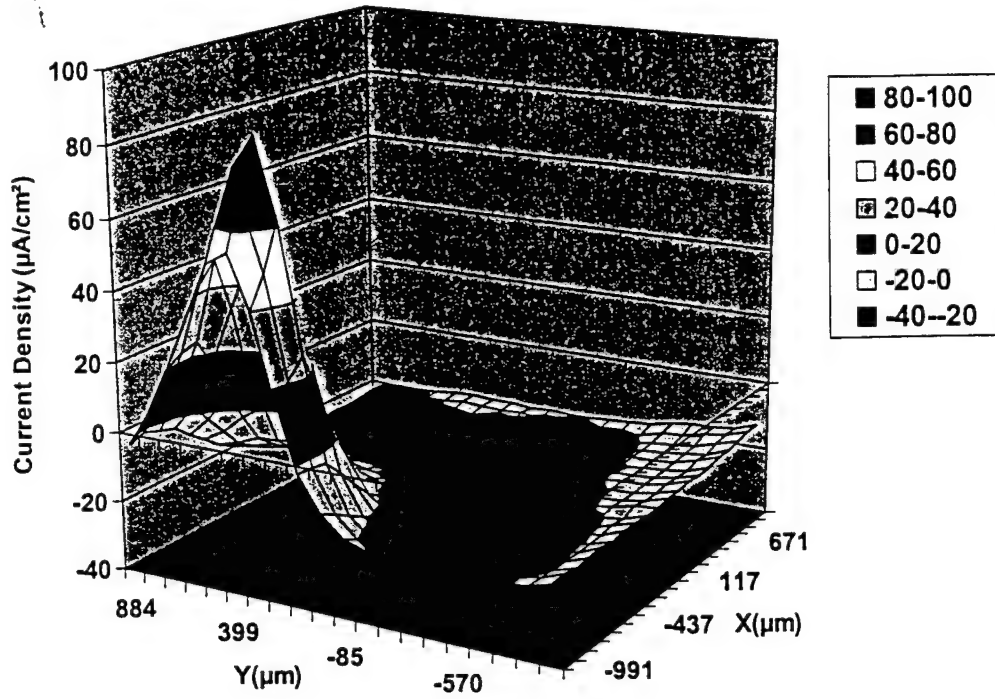
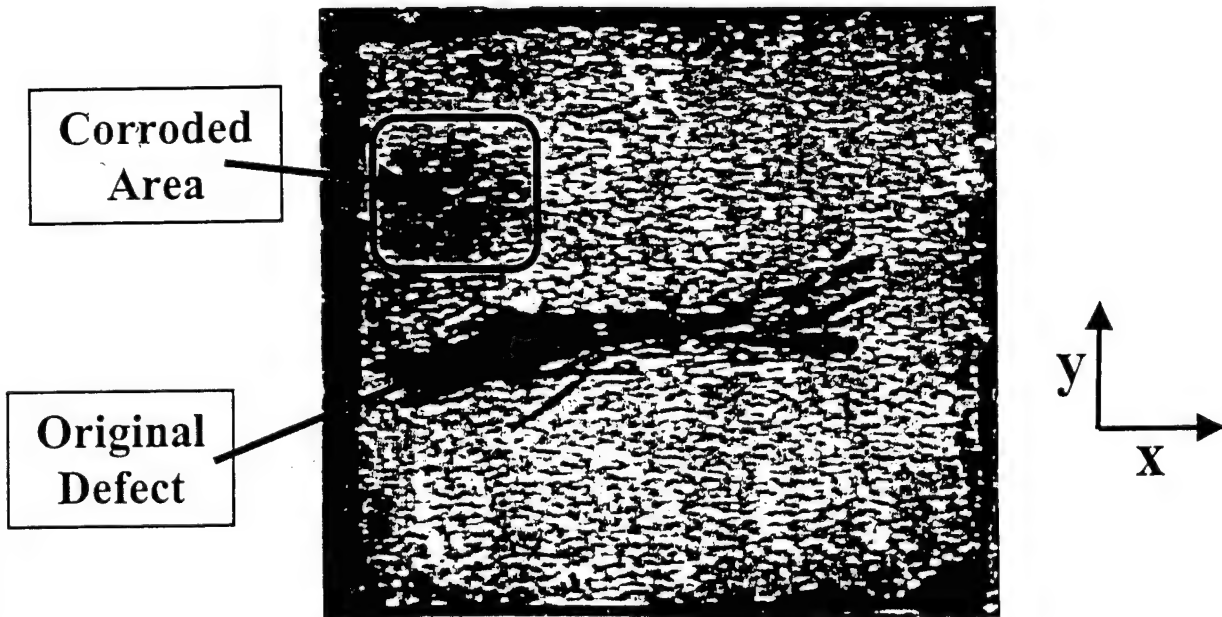


Figure 12



**After removal of the POP coating:**



**Figure 13**

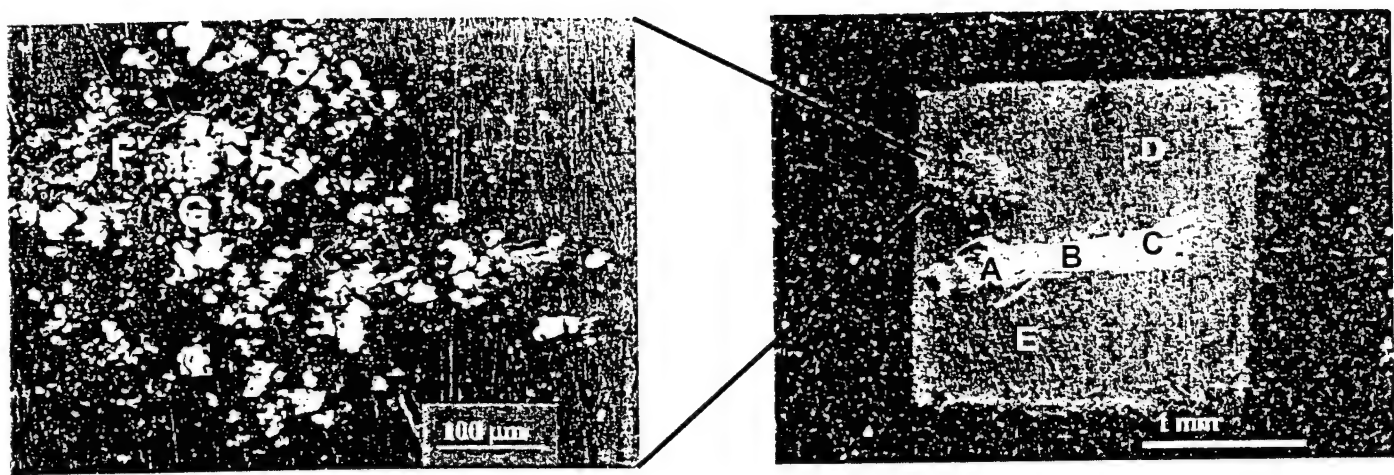
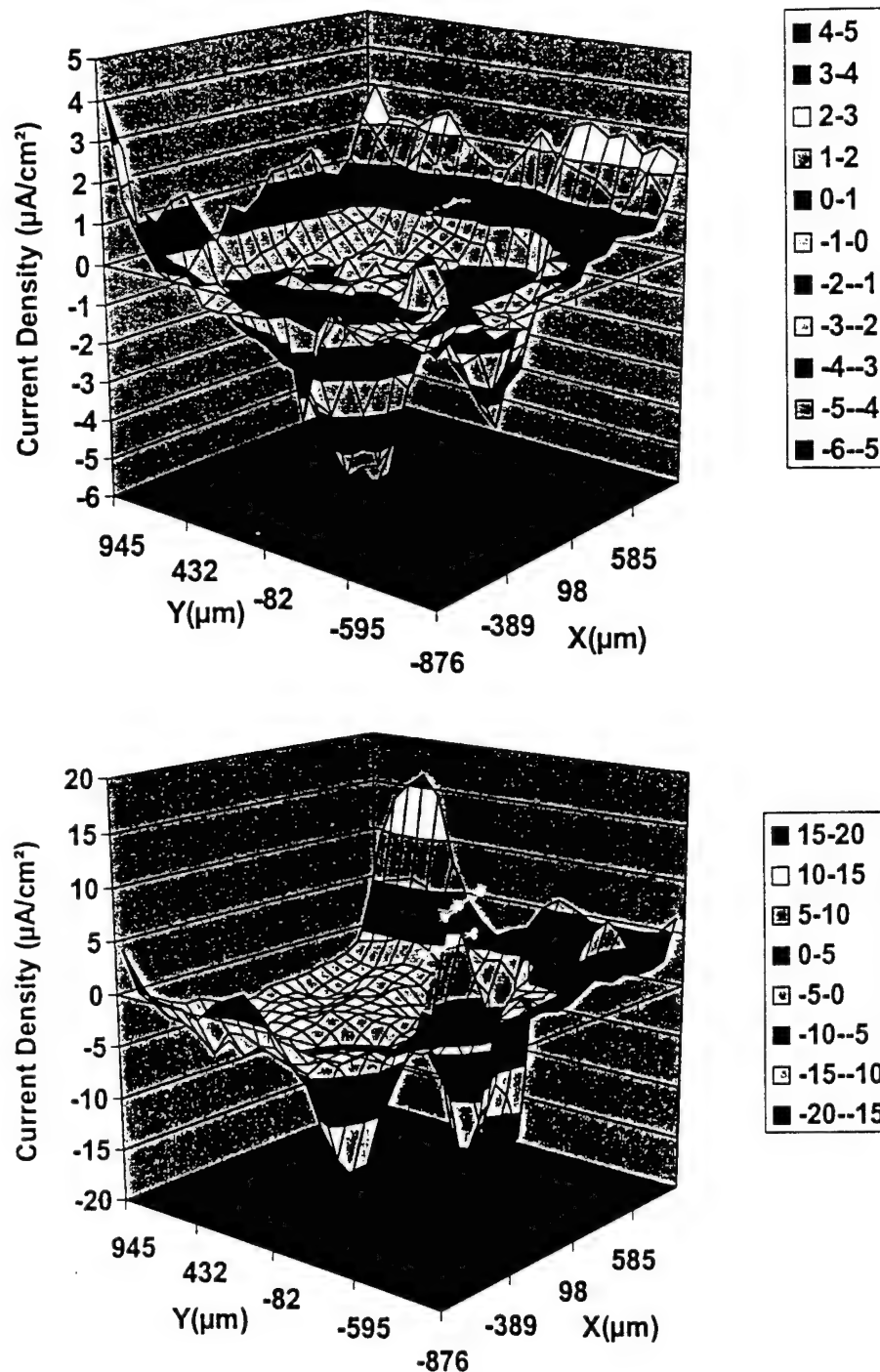
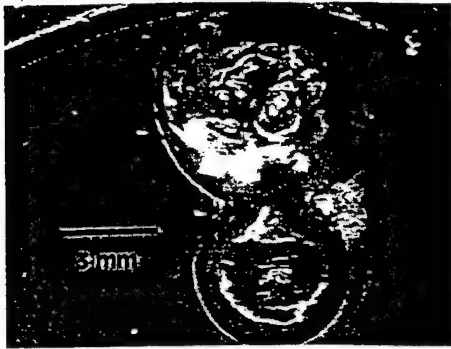


Figure 14



**Figure 15**

Optical micrograph of Polyurethane/Cr-Epoxy/Al 2024-T3



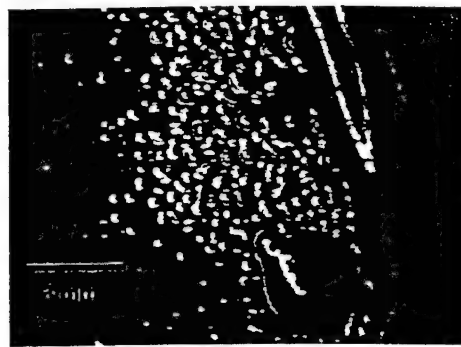
a

Optical micrograph of Polyurethane/POP/Al 2024-T3



b

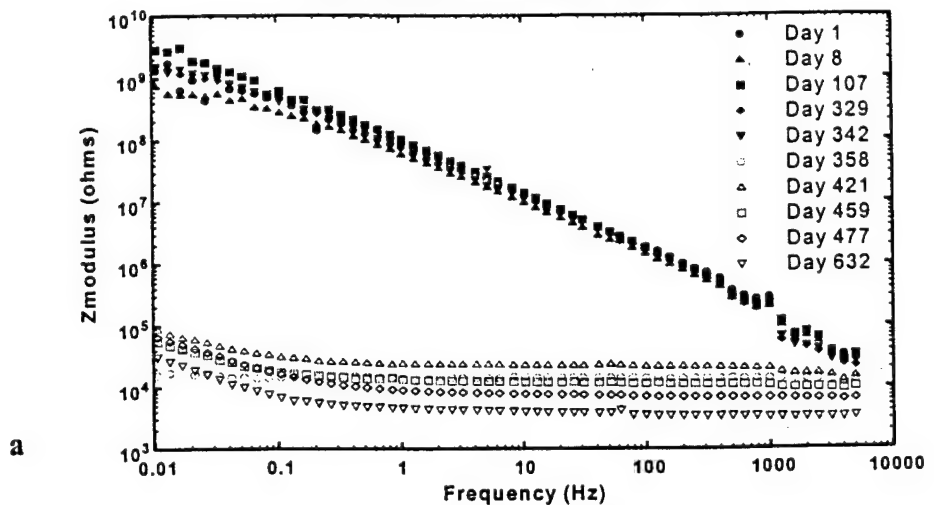
Optical micrograph of Polyurethane/PODP/Al 2024-T3



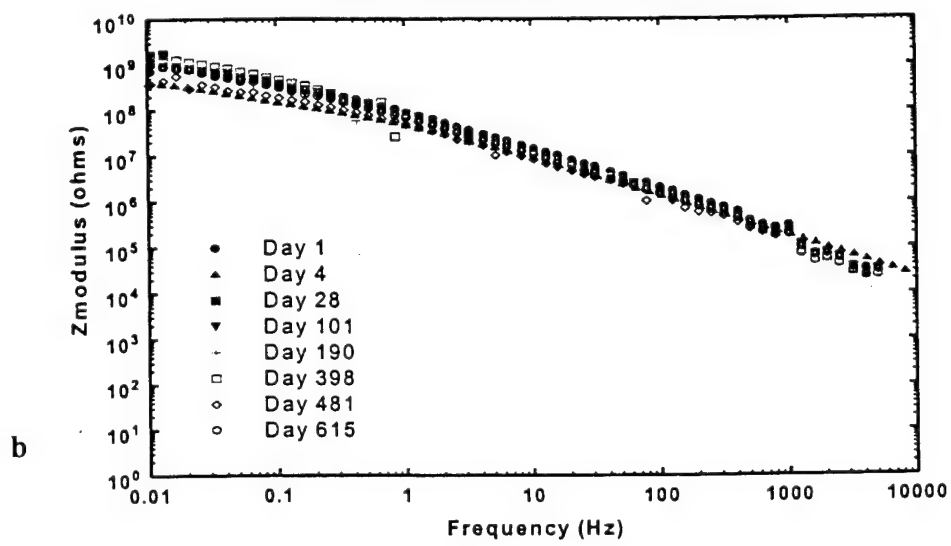
c

**Figures 16a, 16b, and 16c**

Polyurethane/Cr-Epoxy/Al 2024 T-3



Polyurethane/POP/Al 2024 T-3



Figures 17a and 17b

Polyurethane/PODP/Al 2024 T-3

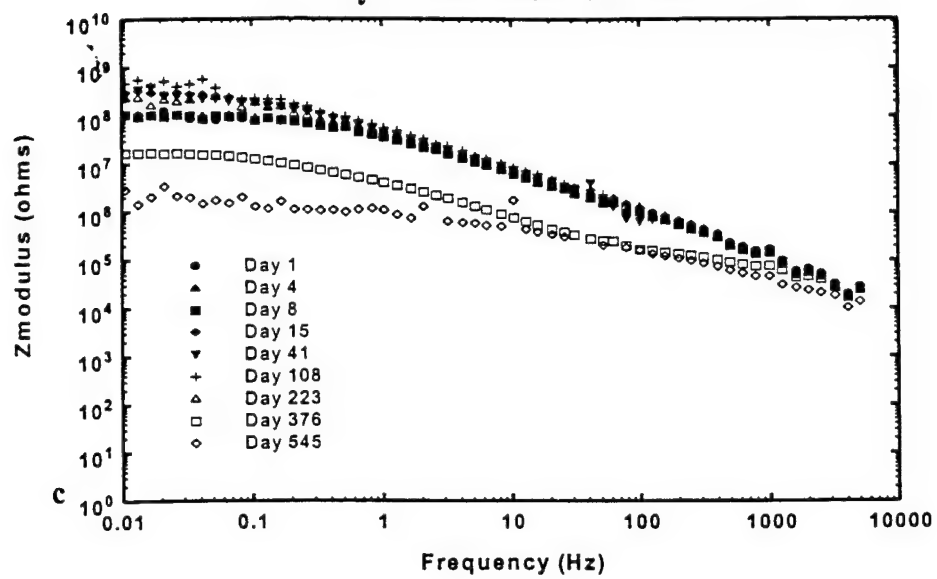
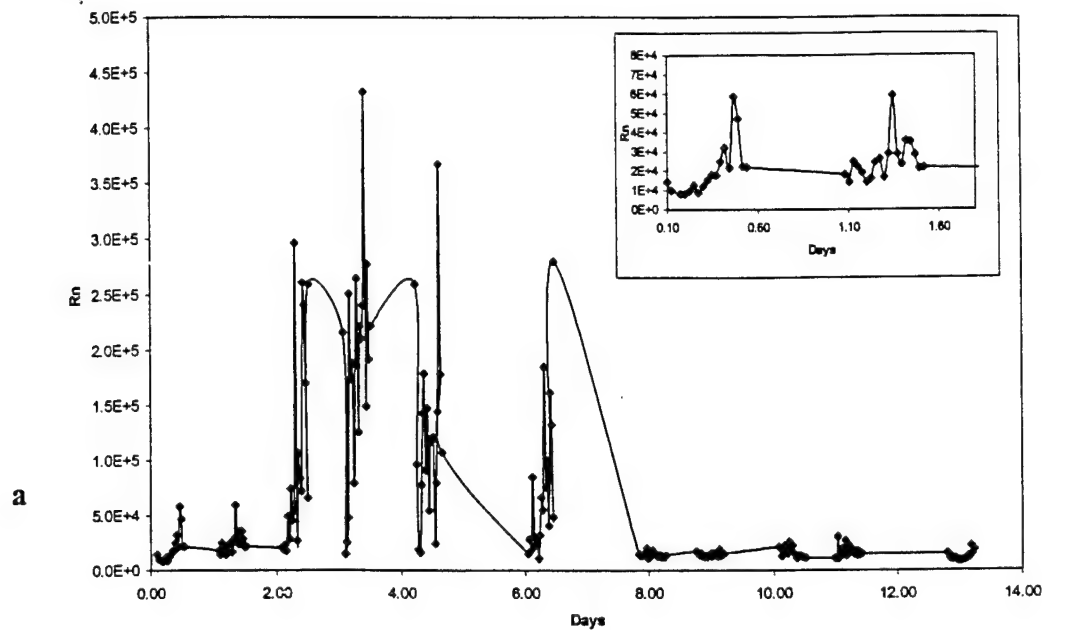
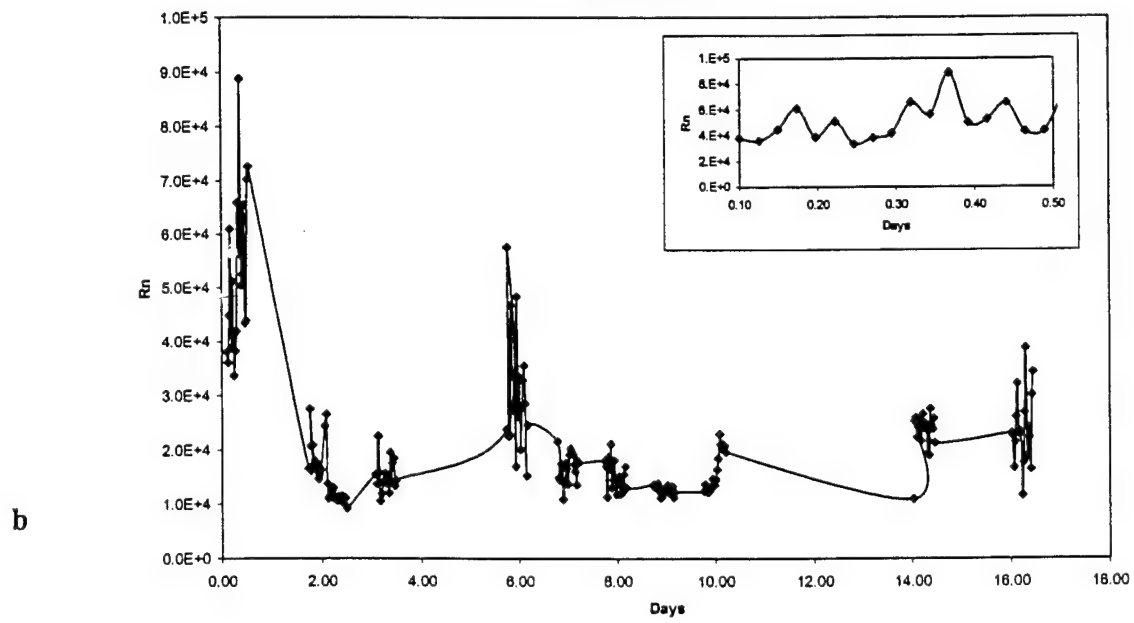


Figure 17c

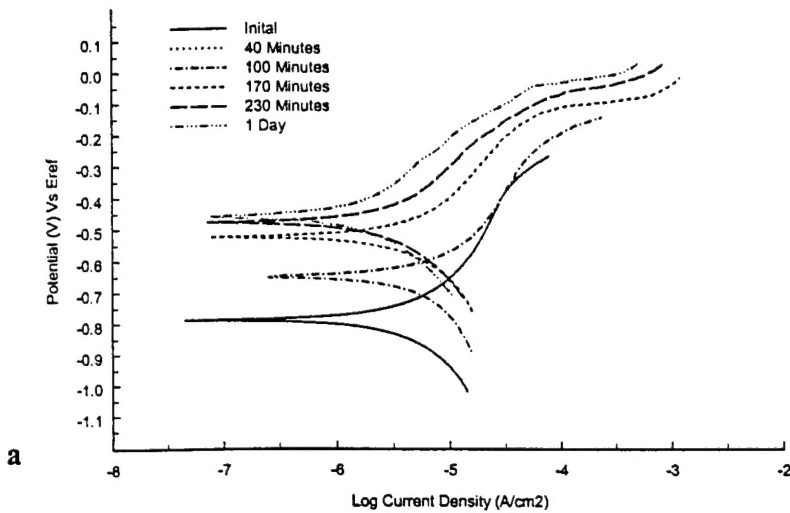
PODP/AI 2024-T3



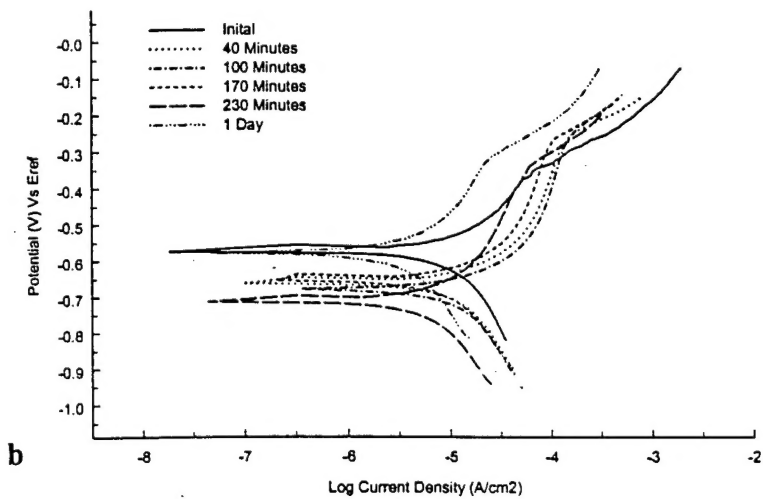
POP/AI 2024-T3

**Figure 18a and 18b**

**POP/AI 2024-T3**



**PODP/AI 2024-T3**



**Figures 19a and 19b**

## pH versus Immersion Time

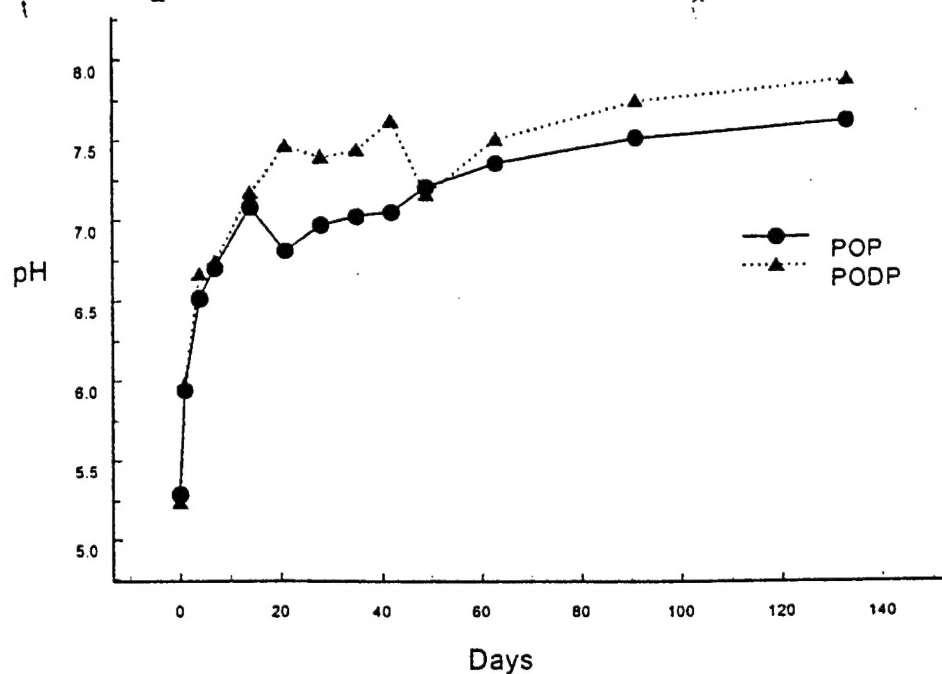
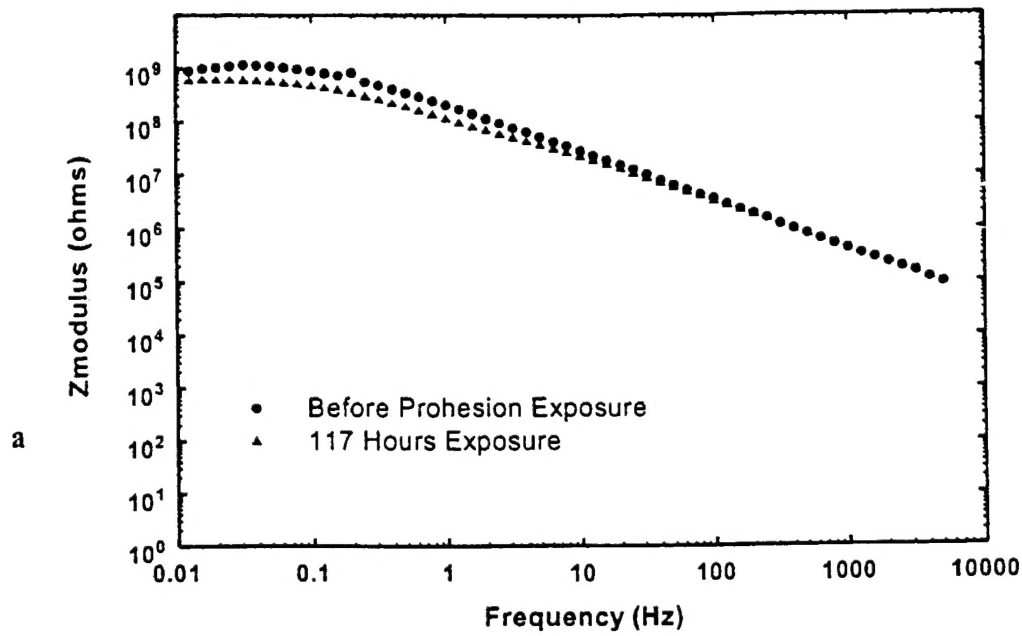
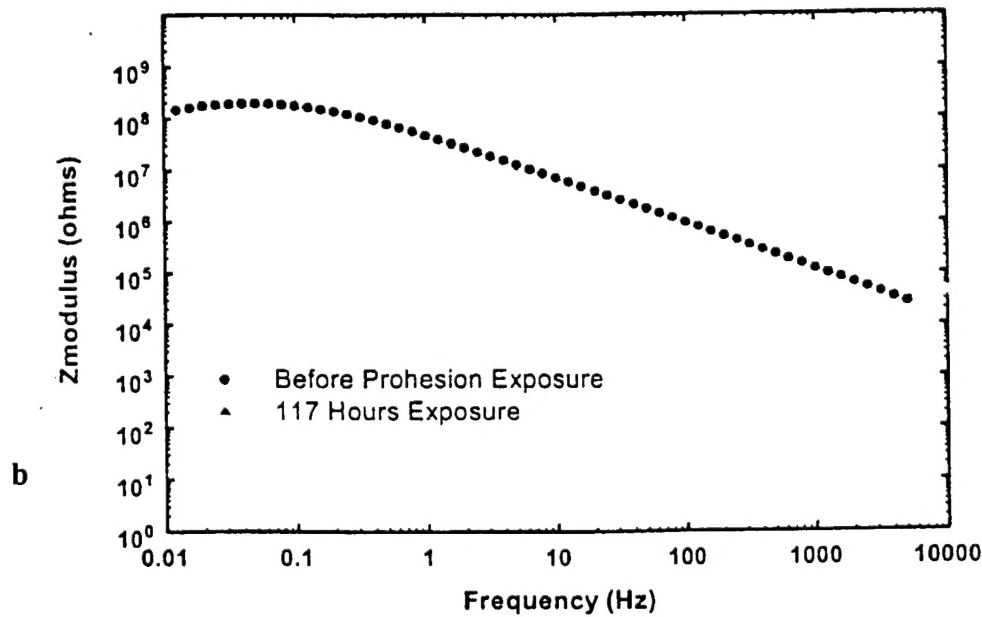


Figure 20

### Polyurethane/Cr-Epoxy/Al 2024-T3



### Polyurethane/PODP/Al 2024-T3



Figures 21a and 21b

### Polyurethane/POP/AI 2024-T3

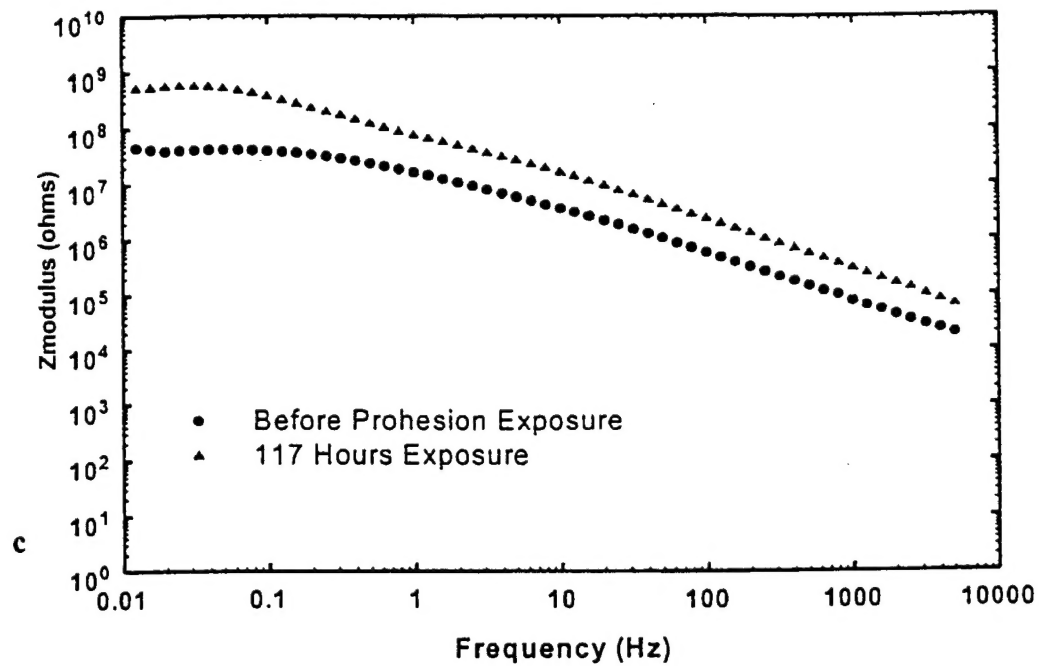


Figure 21c